

Study of $b \rightarrow u\ell\bar{\nu}$ Decays on the Recoil of Fully Reconstructed B Mesons and Determination of $|V_{ub}|$

The BABAR Collaboration

July 16, 2004

Abstract

Based on 88 million $\Upsilon(4S) \rightarrow B\bar{B}$ decays collected by the BABAR experiment at the PEP-II asymmetric-energy B factory at SLAC, we report preliminary results of four analyses which investigate semileptonic charmless B decays, $\bar{B} \rightarrow X_u\ell\bar{\nu}$. Deeper understanding of all aspects of these decays will improve the determination of the Cabibbo-Kobayashi-Maskawa matrix element $|V_{ub}|$. In events in which one B meson decay to a hadronic final state is fully reconstructed, the semileptonic decay of the second B meson is identified by the detection of a charged lepton. By measuring the spectrum of the invariant mass of the hadronic system X_u (M_X), we derive the branching fraction $\mathcal{B}(\bar{B} \rightarrow X_u\ell\bar{\nu}) = (2.53 \pm 0.29(\text{stat.}) \pm 0.26(\text{sys.})_{-0.41}^{+0.69}(\text{theo.})) \times 10^{-3}$. The two-dimensional distribution of M_X and q^2 , the squared lepton-neutrino invariant mass, is used to derive the partial branching fraction for $M_X < 1.7 \text{ GeV}/c^2, q^2 > 8 \text{ GeV}^2/c^4$ to be $\Delta\mathcal{B}(\bar{B} \rightarrow X_u\ell\bar{\nu}) = (0.88 \pm 0.14(\text{stat.}) \pm 0.13(\text{sys.}) \pm 0.02(\text{theo.})) \times 10^{-3}$. From these two measurements we can extract $|V_{ub}| = (4.77 \pm 0.28(\text{stat.}) \pm 0.28(\text{sys.})_{-0.45}^{+0.69}(\text{theo.})) \times 10^{-3}$ and $|V_{ub}| = (4.92 \pm 0.39(\text{stat.}) \pm 0.36(\text{sys.}) \pm 0.46(\text{theo.})) \times 10^{-3}$, respectively. We use the same sample to extract the true M_X distribution for $\bar{B} \rightarrow X_u\ell\bar{\nu}$ events, with the goal of comparing it with theoretical models. We also identify several exclusive charmless semileptonic B decays, and measure the branching fractions $\mathcal{B}(\bar{B} \rightarrow \pi\ell\bar{\nu}) = (1.08 \pm 0.28(\text{stat.}) \pm 0.16(\text{sys.})) \times 10^{-4}$ and $\mathcal{B}(\bar{B} \rightarrow \rho\ell\bar{\nu}) = (2.57 \pm 0.52(\text{stat.}) \pm 0.59(\text{sys.})) \times 10^{-4}$ using isospin and quark model constraints. We also set limits on $\mathcal{B}(B^- \rightarrow \eta\ell\bar{\nu})$, $\mathcal{B}(B^- \rightarrow \eta'\ell\bar{\nu})$, $\mathcal{B}(B^- \rightarrow a_0^0\ell\bar{\nu})\mathcal{B}(a_0^0 \rightarrow \eta\pi^0)$, and $\mathcal{B}(\bar{B}^0 \rightarrow a_0^+\ell\bar{\nu})\mathcal{B}(a_0^+ \rightarrow \eta\pi^+)$.

Submitted to the 32nd International Conference on High-Energy Physics, ICHEP 04,
16 August—22 August 2004, Beijing, China

Stanford Linear Accelerator Center, Stanford University, Stanford, CA 94309

Work supported in part by Department of Energy contract DE-AC03-76SF00515.

The BABAR Collaboration,

B. Aubert, R. Barate, D. Boutigny, F. Couderc, J.-M. Gaillard, A. Hicheur, Y. Karyotakis, J. P. Lees,
V. Tisserand, A. Zghiche

Laboratoire de Physique des Particules, F-74941 Annecy-le-Vieux, France

A. Palano, A. Pompili

Università di Bari, Dipartimento di Fisica and INFN, I-70126 Bari, Italy

J. C. Chen, N. D. Qi, G. Rong, P. Wang, Y. S. Zhu

Institute of High Energy Physics, Beijing 100039, China

G. Eigen, I. Ofte, B. Stugu

University of Bergen, Inst. of Physics, N-5007 Bergen, Norway

G. S. Abrams, A. W. Borgland, A. B. Breon, D. N. Brown, J. Button-Shafer, R. N. Cahn, E. Charles,
C. T. Day, M. S. Gill, A. V. Gritsan, Y. Groysman, R. G. Jacobsen, R. W. Kadel, J. Kadyk, L. T. Kerth,
Yu. G. Kolomensky, G. Kukartsev, G. Lynch, L. M. Mir, P. J. Oddone, T. J. Orimoto, M. Pripstein,
N. A. Roe, M. T. Ronan, V. G. Shelkov, W. A. Wenzel

Lawrence Berkeley National Laboratory and University of California, Berkeley, CA 94720, USA

M. Barrett, K. E. Ford, T. J. Harrison, A. J. Hart, C. M. Hawkes, S. E. Morgan, A. T. Watson

University of Birmingham, Birmingham, B15 2TT, United Kingdom

M. Fritsch, K. Goetzen, T. Held, H. Koch, B. Lewandowski, M. Pelizaeus, M. Steinke
Ruhr Universität Bochum, Institut für Experimentalphysik 1, D-44780 Bochum, Germany

J. T. Boyd, N. Chevalier, W. N. Cottingham, M. P. Kelly, T. E. Latham, F. F. Wilson

University of Bristol, Bristol BS8 1TL, United Kingdom

T. Cuhadar-Donszelmann, C. Hearty, N. S. Knecht, T. S. Mattison, J. A. McKenna, D. Thiessen

University of British Columbia, Vancouver, BC, Canada V6T 1Z1

A. Khan, P. Kyberd, L. Teodorescu

Brunel University, Uxbridge, Middlesex UB8 3PH, United Kingdom

A. E. Blinov, V. E. Blinov, V. P. Druzhinin, V. B. Golubev, V. N. Ivanchenko, E. A. Kravchenko,
A. P. Onuchin, S. I. Serednyakov, Yu. I. Skovpen, E. P. Solodov, A. N. Yushkov

Budker Institute of Nuclear Physics, Novosibirsk 630090, Russia

D. Best, M. Bruinsma, M. Chao, I. Eschrich, D. Kirkby, A. J. Lankford, M. Mandelkern, R. K. Mommsen,
W. Roethel, D. P. Stoker

University of California at Irvine, Irvine, CA 92697, USA

C. Buchanan, B. L. Hartfiel

University of California at Los Angeles, Los Angeles, CA 90024, USA

S. D. Foulkes, J. W. Gary, B. C. Shen, K. Wang

University of California at Riverside, Riverside, CA 92521, USA

- D. del Re, H. K. Hadavand, E. J. Hill, D. B. MacFarlane, H. P. Paar, Sh. Rahatlou, V. Sharma
University of California at San Diego, La Jolla, CA 92093, USA
- J. W. Berryhill, C. Campagnari, B. Dahmes, O. Long, A. Lu, M. A. Mazur, J. D. Richman, W. Verkerke
University of California at Santa Barbara, Santa Barbara, CA 93106, USA
- T. W. Beck, A. M. Eisner, C. A. Heusch, J. Kroseberg, W. S. Lockman, G. Nesom, T. Schalk,
 B. A. Schumm, A. Seiden, P. Spradlin, D. C. Williams, M. G. Wilson
University of California at Santa Cruz, Institute for Particle Physics, Santa Cruz, CA 95064, USA
- J. Albert, E. Chen, G. P. Dubois-Felsmann, A. Dvoretzskii, D. G. Hitlin, I. Narsky, T. Piatenko,
 F. C. Porter, A. Ryd, A. Samuel, S. Yang
California Institute of Technology, Pasadena, CA 91125, USA
- S. Jayatilleke, G. Mancinelli, B. T. Meadows, M. D. Sokoloff
University of Cincinnati, Cincinnati, OH 45221, USA
- T. Abe, F. Blanc, P. Bloom, S. Chen, W. T. Ford, U. Nauenberg, A. Olivas, P. Rankin, J. G. Smith,
 J. Zhang, L. Zhang
University of Colorado, Boulder, CO 80309, USA
- A. Chen, J. L. Harton, A. Soffer, W. H. Toki, R. J. Wilson, Q. Zeng
Colorado State University, Fort Collins, CO 80523, USA
- D. Altenburg, T. Brandt, J. Brose, M. Dickopp, E. Feltresi, A. Hauke, H. M. Lacker, R. Müller-Pfefferkorn,
 R. Nogowski, S. Otto, A. Petzold, J. Schubert, K. R. Schubert, R. Schwierz, B. Spaan, J. E. Sundermann,
 K. Tackmann
Technische Universität Dresden, Institut für Kern- und Teilchenphysik, D-01062 Dresden, Germany
- D. Bernard, G. R. Bonneaud, F. Brochard, P. Grenier, S. Schrenk, Ch. Thiebaux, G. Vasileiadis, M. Verderi
Ecole Polytechnique, LLR, F-91128 Palaiseau, France
- D. J. Bard, P. J. Clark, D. Lavin, F. Muheim, S. Playfer, Y. Xie
University of Edinburgh, Edinburgh EH9 3JZ, United Kingdom
- M. Andreotti, V. Azzolini, D. Bettoni, C. Bozzi, R. Calabrese, G. Cibinetto, E. Luppi, M. Negrini,
 L. Piemontese, A. Sarti
Università di Ferrara, Dipartimento di Fisica and INFN, I-44100 Ferrara, Italy
- E. Treadwell
Florida A&M University, Tallahassee, FL 32307, USA
- F. Anulli, R. Baldini-Ferroli, A. Calcaterra, R. de Sangro, G. Finocchiaro, P. Patteri, I. M. Peruzzi,
 M. Piccolo, A. Zallo
Laboratori Nazionali di Frascati dell'INFN, I-00044 Frascati, Italy
- A. Buzzo, R. Capra, R. Contri, G. Crosetti, M. Lo Vetere, M. Macri, M. R. Monge, S. Passaggio,
 C. Patrignani, E. Robutti, A. Santroni, S. Tosi
Università di Genova, Dipartimento di Fisica and INFN, I-16146 Genova, Italy

S. Bailey, G. Brandenburg, K. S. Chaisanguanthum, M. Morii, E. Won
Harvard University, Cambridge, MA 02138, USA

R. S. Dubitzky, U. Langenegger
Universität Heidelberg, Physikalisches Institut, Philosophenweg 12, D-69120 Heidelberg, Germany

W. Bhimji, D. A. Bowerman, P. D. Dauncey, U. Egede, J. R. Gaillard, G. W. Morton, J. A. Nash,
M. B. Nikolich, G. P. Taylor
Imperial College London, London, SW7 2AZ, United Kingdom

M. J. Charles, G. J. Grenier, U. Mallik
University of Iowa, Iowa City, IA 52242, USA

J. Cochran, H. B. Crawley, J. Lamsa, W. T. Meyer, S. Prell, E. I. Rosenberg, A. E. Rubin, J. Yi
Iowa State University, Ames, IA 50011-3160, USA

M. Biasini, R. Covarelli, M. Pioppi
Università di Perugia, Dipartimento di Fisica and INFN, I-06100 Perugia, Italy

M. Davier, X. Giroux, G. Grosdidier, A. Höcker, S. Laplace, F. Le Diberder, V. Lepeltier, A. M. Lutz,
T. C. Petersen, S. Plaszczynski, M. H. Schune, L. Tantot, G. Wormser
Laboratoire de l'Accélérateur Linéaire, F-91898 Orsay, France

C. H. Cheng, D. J. Lange, M. C. Simani, D. M. Wright
Lawrence Livermore National Laboratory, Livermore, CA 94550, USA

A. J. Bevan, C. A. Chavez, J. P. Coleman, I. J. Forster, J. R. Fry, E. Gabathuler, R. Gamet,
D. E. Hutchcroft, R. J. Parry, D. J. Payne, R. J. Sloane, C. Touramanis
University of Liverpool, Liverpool L69 7ZE, United Kingdom

J. J. Back,¹ C. M. Cormack, P. F. Harrison,¹ F. Di Lodovico, G. B. Mohanty¹
Queen Mary, University of London, E1 4NS, United Kingdom

C. L. Brown, G. Cowan, R. L. Flack, H. U. Flaecher, M. G. Green, P. S. Jackson, T. R. McMahon,
S. Ricciardi, F. Salvatore, M. A. Winter
*University of London, Royal Holloway and Bedford New College, Egham, Surrey TW20 0EX,
United Kingdom*

D. Brown, C. L. Davis
University of Louisville, Louisville, KY 40292, USA

J. Allison, N. R. Barlow, R. J. Barlow, P. A. Hart, M. C. Hodgkinson, G. D. Lafferty, A. J. Lyon,
J. C. Williams
University of Manchester, Manchester M13 9PL, United Kingdom

A. Farbin, W. D. Hulsbergen, A. Jawahery, D. Kovalskyi, C. K. Lae, V. Lillard, D. A. Roberts
University of Maryland, College Park, MD 20742, USA

¹Now at Department of Physics, University of Warwick, Coventry, United Kingdom

G. Blaylock, C. Dallapiccola, K. T. Flood, S. S. Hertzbach, R. Kofler, V. B. Koptchev, T. B. Moore,
S. Saremi, H. Staengle, S. Willocq

University of Massachusetts, Amherst, MA 01003, USA

R. Cowan, G. Sciolla, S. J. Sekula, F. Taylor, R. K. Yamamoto

Massachusetts Institute of Technology, Laboratory for Nuclear Science, Cambridge, MA 02139, USA

D. J. J. Mangeol, P. M. Patel, S. H. Robertson

McGill University, Montréal, QC, Canada H3A 2T8

A. Lazzaro, V. Lombardo, F. Palombo

Università di Milano, Dipartimento di Fisica and INFN, I-20133 Milano, Italy

J. M. Bauer, L. Cremaldi, V. Eschenburg, R. Godang, R. Kroeger, J. Reidy, D. A. Sanders, D. J. Summers,
H. W. Zhao

University of Mississippi, University, MS 38677, USA

S. Brunet, D. Côté, P. Taras

Université de Montréal, Laboratoire René J. A. Lévesque, Montréal, QC, Canada H3C 3J7

H. Nicholson

Mount Holyoke College, South Hadley, MA 01075, USA

N. Cavallo,² F. Fabozzi,² C. Gatto, L. Lista, D. Monorchio, P. Paolucci, D. Piccolo, C. Sciacca
Università di Napoli Federico II, Dipartimento di Scienze Fisiche and INFN, I-80126, Napoli, Italy

M. Baak, H. Bulten, G. Raven, H. L. Snoek, L. Wilden

*NIKHEF, National Institute for Nuclear Physics and High Energy Physics, NL-1009 DB Amsterdam,
The Netherlands*

C. P. Jessop, J. M. LoSecco

University of Notre Dame, Notre Dame, IN 46556, USA

T. Allmendinger, K. K. Gan, K. Honscheid, D. Hufnagel, H. Kagan, R. Kass, T. Pulliam, A. M. Rahimi,
R. Ter-Antonyan, Q. K. Wong

Ohio State University, Columbus, OH 43210, USA

J. Brau, R. Frey, O. Igonkina, C. T. Potter, N. B. Sinev, D. Strom, E. Torrence

University of Oregon, Eugene, OR 97403, USA

F. Colecchia, A. Dorigo, F. Galeazzi, M. Margoni, M. Morandin, M. Posocco, M. Rotondo, F. Simonetto,
R. Stroili, G. Tiozzo, C. Voci

Università di Padova, Dipartimento di Fisica and INFN, I-35131 Padova, Italy

M. Benayoun, H. Briand, J. Chauveau, P. David, Ch. de la Vaissière, L. Del Buono, O. Hamon,
M. J. J. John, Ph. Leruste, J. Malcles, J. Ocariz, M. Pivk, L. Roos, S. T'Jampens, G. Therin

*Universités Paris VI et VII, Laboratoire de Physique Nucléaire et de Hautes Energies, F-75252 Paris,
France*

²Also with Università della Basilicata, Potenza, Italy

P. F. Manfredi, V. Re

Università di Pavia, Dipartimento di Elettronica and INFN, I-27100 Pavia, Italy

P. K. Behera, L. Gladney, Q. H. Guo, J. Panetta

University of Pennsylvania, Philadelphia, PA 19104, USA

C. Angelini, G. Batignani, S. Bettarini, M. Bondioli, F. Bucci, G. Calderini, M. Carpinelli, F. Forti,
M. A. Giorgi, A. Lusiani, G. Marchiori, F. Martinez-Vidal,³ M. Morganti, N. Neri, E. Paoloni, M. Rama,
G. Rizzo, F. Sandrelli, J. Walsh

Università di Pisa, Dipartimento di Fisica, Scuola Normale Superiore and INFN, I-56127 Pisa, Italy

M. Haire, D. Judd, K. Paick, D. E. Wagoner

Prairie View A&M University, Prairie View, TX 77446, USA

N. Danielson, P. Elmer, Y. P. Lau, C. Lu, V. Miftakov, J. Olsen, A. J. S. Smith, A. V. Telnov

Princeton University, Princeton, NJ 08544, USA

F. Bellini, G. Cavoto,⁴ R. Faccini, F. Ferrarotto, F. Ferroni, M. Gaspero, L. Li Gioi, M. A. Mazzoni,
S. Morganti, M. Pierini, G. Piredda, F. Safai Tehrani, C. Voena

Università di Roma La Sapienza, Dipartimento di Fisica and INFN, I-00185 Roma, Italy

S. Christ, G. Wagner, R. Walldi

Universität Rostock, D-18051 Rostock, Germany

T. Adye, N. De Groot, B. Franek, N. I. Geddes, G. P. Gopal, E. O. Olaiya

Rutherford Appleton Laboratory, Chilton, Didcot, Oxon, OX11 0QX, United Kingdom

R. Aleksan, S. Emery, A. Gaidot, S. F. Ganzhur, P.-F. Giraud, G. Hamel de Monchenault, W. Kozanecki,
M. Legendre, G. W. London, B. Mayer, G. Schott, G. Vasseur, Ch. Yèche, M. Zito

DSM/Daphnia, CEA/Saclay, F-91191 Gif-sur-Yvette, France

M. V. Purohit, A. W. Weidemann, J. R. Wilson, F. X. Yumiceva

University of South Carolina, Columbia, SC 29208, USA

D. Aston, R. Bartoldus, N. Berger, A. M. Boyarski, O. L. Buchmueller, R. Claus, M. R. Convery,
M. Cristinziani, G. De Nardo, D. Dong, J. Dorfan, D. Dujmic, W. Dunwoodie, E. E. Elsen, S. Fan,
R. C. Field, T. Glanzman, S. J. Gowdy, T. Hadig, V. Halyo, C. Hast, T. Hryn'ova, W. R. Innes,
M. H. Kelsey, P. Kim, M. L. Kocian, D. W. G. S. Leith, J. Libby, S. Luitz, V. Luth, H. L. Lynch,
H. Marsiske, R. Messner, D. R. Muller, C. P. O'Grady, V. E. Ozcan, A. Perazzo, M. Perl, S. Petrak,
B. N. Ratcliff, A. Roodman, A. A. Salnikov, R. H. Schindler, J. Schwiening, G. Simi, A. Snyder, A. Soha,
J. Stelzer, D. Su, M. K. Sullivan, J. Va'vra, S. R. Wagner, M. Weaver, A. J. R. Weinstein,
W. J. Wisniewski, M. Wittgen, D. H. Wright, A. K. Yarritu, C. C. Young

Stanford Linear Accelerator Center, Stanford, CA 94309, USA

P. R. Burchat, A. J. Edwards, T. I. Meyer, B. A. Petersen, C. Roat

Stanford University, Stanford, CA 94305-4060, USA

³Also with IFIC, Instituto de Física Corpuscular, CSIC-Universidad de Valencia, Valencia, Spain

⁴Also with Princeton University, Princeton, USA

S. Ahmed, M. S. Alam, J. A. Ernst, M. A. Saeed, M. Saleem, F. R. Wappler
State University of New York, Albany, NY 12222, USA

W. Bugg, M. Krishnamurthy, S. M. Spanier
University of Tennessee, Knoxville, TN 37996, USA

R. Eckmann, H. Kim, J. L. Ritchie, A. Satpathy, R. F. Schwitters
University of Texas at Austin, Austin, TX 78712, USA

J. M. Izen, I. Kitayama, X. C. Lou, S. Ye
University of Texas at Dallas, Richardson, TX 75083, USA

F. Bianchi, M. Bona, F. Gallo, D. Gamba
Università di Torino, Dipartimento di Fisica Sperimentale and INFN, I-10125 Torino, Italy

L. Bosisio, C. Cartaro, F. Cossutti, G. Della Ricca, S. Dittongo, S. Grancagnolo, L. Lanceri, P. Poropat,⁵
L. Vitale, G. Vuagnin
Università di Trieste, Dipartimento di Fisica and INFN, I-34127 Trieste, Italy

R. S. Panvini
Vanderbilt University, Nashville, TN 37235, USA

Sw. Banerjee, C. M. Brown, D. Fortin, P. D. Jackson, R. Kowalewski, J. M. Roney, R. J. Sobie
University of Victoria, Victoria, BC, Canada V8W 3P6

H. R. Band, B. Cheng, S. Dasu, M. Datta, A. M. Eichenbaum, M. Graham, J. J. Hollar, J. R. Johnson,
P. E. Kutter, H. Li, R. Liu, A. Mihalyi, A. K. Mohapatra, Y. Pan, R. Prepost, P. Tan, J. H. von
Wimmersperg-Toeller, J. Wu, S. L. Wu, Z. Yu
University of Wisconsin, Madison, WI 53706, USA

M. G. Greene, H. Neal
Yale University, New Haven, CT 06511, USA

⁵Deceased

1 Introduction

The principal physics goal of the *BABAR* experiment is to establish CP violation in B mesons and to test whether the observed effects are consistent with the predictions of the Standard Model (SM). CP violating effects result in the SM from an irreducible phase in the Cabibbo-Kobayashi-Maskawa (CKM) matrix which describes the couplings of the charged weak current to quarks. An improved determination of the absolute value of the matrix element $|V_{ub}|$, the coupling strength of the b quark to the u quark, will contribute critically to tests of the consistency of the angles of the unitarity triangle of the CKM matrix.

The extraction of $|V_{ub}|$ is a challenge both for theory and experiment. Experimentally, the main problem is the separation of $b \rightarrow ul\nu$ decays from the more abundant $b \rightarrow cl\nu$ decays. Selection criteria applied to achieve this separation generally make the theoretical extrapolation to the full decay rate more difficult. Theoretically, inclusive semileptonic rates can be calculated reliably at the parton level. However, the dynamics of B meson decays depend on the b quark mass and its motion inside the meson. Calculations of the decay rate rely on operator product expansions (OPE) in inverse powers of the b quark mass. These depend on the choice of renormalization scale and include non-perturbative contributions, resummed into the so-called shape function (SF), which introduce model uncertainties. Exclusive branching fractions can also be related to $|V_{ub}|$, although with large errors. In addition, the as yet poorly known dynamics of the decays introduce large uncertainties in the determination of the efficiencies of the selection criteria. To reduce these uncertainties we apply as loose selection criteria as possible to exclusive $\bar{B} \rightarrow X_u \ell \bar{\nu}$ decays⁶.

At the $\Upsilon(4S)$ resonance, events with a reconstructed B decay to hadronic final states are an optimal environment for the study of semileptonic decays of the second B meson. The relatively small backgrounds allow for loose selection criteria and reduce the uncertainty in the extrapolation to the full decay rate. Moreover, the fact that the B momentum is known allows us to isolate the signal in several regions of phase space and perform different measurements with relatively uncorrelated theoretical and experimental uncertainties. The kinematic variables considered in this paper are M_X , the invariant mass of the hadrons X , and q^2 , the squared invariant mass of the two leptons. The main background from $\bar{B} \rightarrow X_c \ell \bar{\nu}$ decays is located at high values of M_X and low values of q^2 , while the $\bar{B} \rightarrow X_u \ell \bar{\nu}$ signal events extends to low M_X and high q^2 values (see Fig 1).

In this paper we present several preliminary results that extend the $|V_{ub}|$ analysis published by *BABAR* in Ref. [1]. These new studies are based on the same analysis strategy and data set. They are motivated by the recent discussion on the theoretical uncertainties to be assigned to the measurement of $|V_{ub}|$, see for instance [2, 3, 4] and by the possibility of studying exclusive charmless decays with high purity. This paper presents four separate results:

- A $|V_{ub}|$ measurement is performed utilizing the M_X spectrum, as in Ref. [1], following the approach from De Fazio and Neubert [5] referred to as “DFN” in the following. An updated estimate of the SF parameters is used for the extrapolation to the full phase space. This analysis will be referred to as the “ M_X ” analysis.
- A determination of the true M_X spectrum with detector effects unfolded (“unfolding” analysis). This spectrum allows for a direct comparison with theoretical models and with more statistics will be able to constrain the SF parameters. We determine the cumulative M_X distribution, as well as the first and second mass moment of the M_X distribution.

⁶Unless otherwise specified, charge conjugation is always implied throughout this paper.

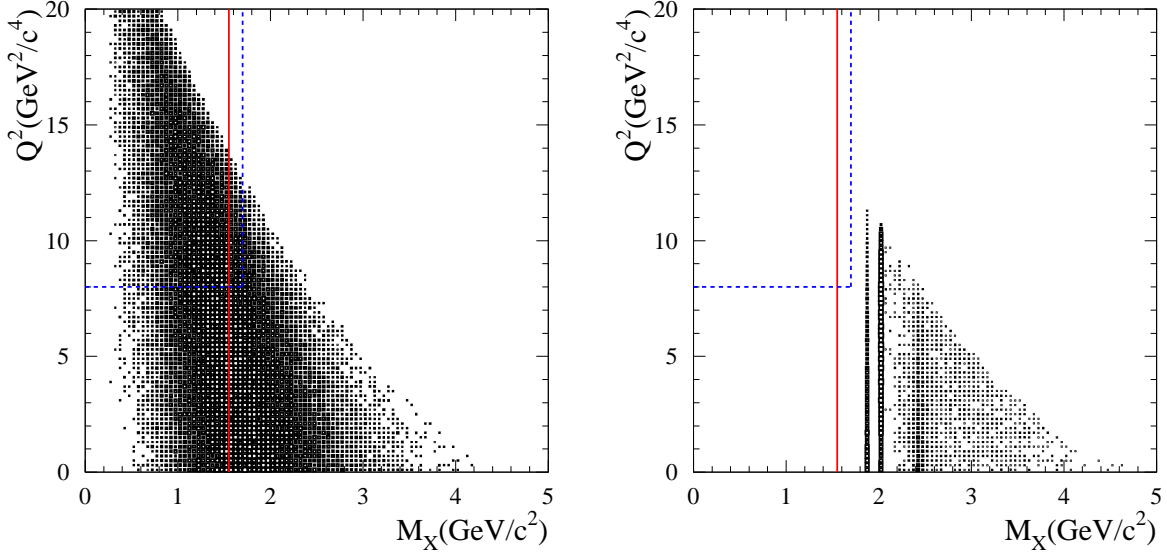


Figure 1: Distribution on MonteCarlo simulated events of the squared invariant mass of the leptons (q^2) and the invariant mass of the hadronic recoil system (M_X) in semileptonic $b \rightarrow u\ell\bar{\nu}$ (left) and $b \rightarrow c\ell\bar{\nu}$ decays (right). The model utilized is the non-resonant model described in Sec. 2.1. The full (dashed) line indicates the phase-space region selected by the $M_X(M_X-q^2)$ analysis.

- A $|V_{ub}|$ measurement is performed by utilizing the two-dimensional distribution of M_X and q^2 and by following the approach of Bauer, Ligeti and Luke [6], referred to as “BLL” in the following. This analysis, which will be referred to as the “ M_X-q^2 ” analysis, requires the determination of the partial branching fraction in limited regions of the phase space.
- A measurement of branching fractions for exclusive charmless semileptonic B decays. In this case the semileptonic decay is identified by a charged lepton, and the hadronic state is exclusively reconstructed. We analyze the following decay modes: $\bar{B}^0 \rightarrow \pi^+\ell\bar{\nu}$, $B^- \rightarrow \pi^0\ell\bar{\nu}$, $\bar{B}^0 \rightarrow \rho^+\ell\bar{\nu}$, $B^- \rightarrow \rho^0\ell\bar{\nu}$, $B^- \rightarrow \omega\ell\bar{\nu}$, $B^- \rightarrow \eta\ell\bar{\nu}$, $B^- \rightarrow \eta'\ell\bar{\nu}$, $B^- \rightarrow a_0^0\ell\bar{\nu}$ and $\bar{B}^0 \rightarrow a_0^+\ell\bar{\nu}$.

A review of the previous measurements of $|V_{ub}|$ is given in Ref. [4]. The measurements reported here are either based on novel techniques or have smaller uncertainties than the existing ones.

This paper is organized as follows: section 2 describes the detector, the data sample and the Monte Carlo simulation including a description of the theoretical model on which our efficiency calculations are based. Section 3 describes the aspects common to all analyses presented here. Section 4 presents a new interpretation of the published M_X analysis that takes the latest theoretical developments into account. Section 5 discusses the results of the M_X spectrum unfolding (on the whole q^2 range). Section 6 shows the details and the results of the M_X-q^2 analysis, while Section 7 shows the results for an alternative set of SF parameters. Finally in Section 8 we present the measurement of exclusive $\bar{B} \rightarrow X_u\ell\bar{\nu}$ branching fractions.

2 Data Sample and Simulation

The data used in this paper were recorded with the *BABAR* detector [7] at the PEP-II collider in the period October 1999–September 2002. The total integrated luminosity of the data set is 81.9 fb^{-1} collected on the $\Upsilon(4S)$ resonance. The corresponding number of produced $B\bar{B}$ pairs is 88 million. We use Monte Carlo (MC) simulations of the *BABAR* detector based on *GEANT* [8] to optimize selection criteria and to determine signal efficiencies and background distributions.

2.1 Simulation of $\bar{B} \rightarrow X_u \ell \bar{\nu}$ decays

Charmless semileptonic $\bar{B} \rightarrow X_u \ell \bar{\nu}$ decays are simulated as a combination of both three-body decays to narrow resonances, $X_u = \pi, \eta, \rho, \omega, \eta'$, and decays to non-resonant hadronic final states X_u .

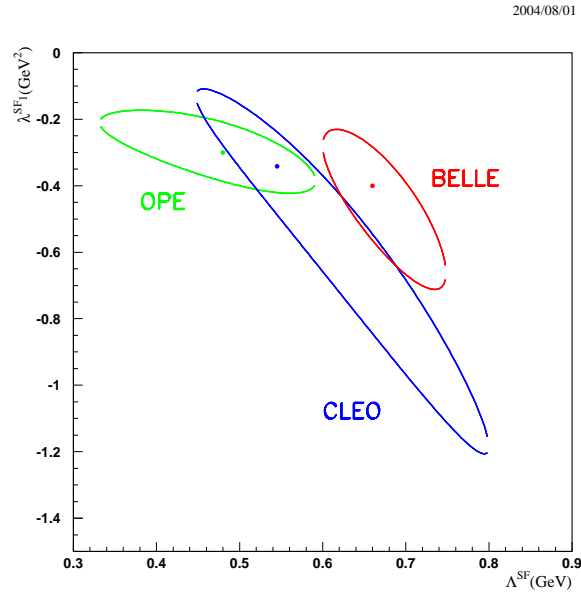


Figure 2: $\Delta\chi^2 = 1$ contours for the fit to $b \rightarrow c\ell\nu$ moments in Ref. [9](green) and the $b \rightarrow s\gamma$ photon energy spectra in Belle [12] (red) and CLEO [4] (blue). Dots represent the best χ^2 points.

The simulation of the inclusive charmless semileptonic B decays into hadronic states with masses larger than $2m_\pi$ is based on a prescription by De Fazio and Neubert [5] (DFN), which calculates the triple differential decay rate, $d^3\Gamma/dq^2 dE_\ell ds_H$ ($s_H = m_X^2$), up to $\mathcal{O}(\alpha_s)$ corrections. The motion of the b quark inside the B meson is incorporated in the DFN formalism by convolving the parton-level triple differential decay rate with a non-perturbative shape function (SF). The SF describes the distribution of the momentum k_+ of the b quark inside the B meson. The two free parameters of the SF are $\bar{\Lambda}^{SF}$ and λ_1^{SF} . The first relates the B meson mass, m_B , to the b quark mass, $m_b^{SF} = m_B - \bar{\Lambda}^{SF}$, and $-\lambda_1^{SF}$ is the average momentum squared of the b quark in the B meson. The SF parameterization used in the generator is of the form

$$F(k_+) = N(1-x)^a e^{(1+a)x}, \quad (1)$$

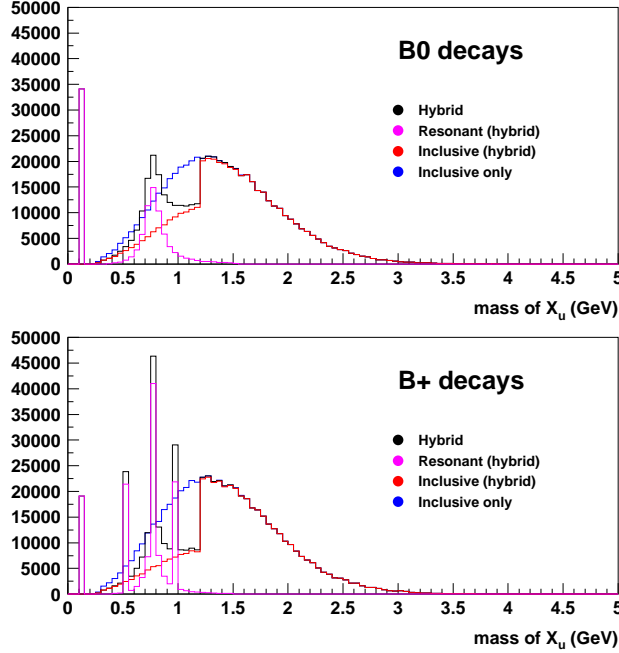


Figure 3: Model for the simulation of $b \rightarrow u\ell\bar{\nu}$ decays for neutral (top) and charged (bottom) B mesons: resonant decays (purple - peaky) are combined with weighted non-resonant (“inclusive”) simulated events (red - smooth) to form the “hybrid” model (black). The inclusive sample is also shown before applying the weights (blue).

where $x = \frac{k_+}{\bar{\Lambda}^{SF}} \leq 1$ and $a = -3(\bar{\Lambda}^{SF})^2/\lambda_1^{SF} - 1$. The original DFN paper [5] suggested that the SF parameters could be related to the operator product expansion parameters by $m_B - \bar{\Lambda}^{SF} = m_b$ and $\lambda_1^{SF} = -\mu_\pi^2$. Since there is currently no consensus on these relationships (see for instance Refs. [2, 3]) we choose to use the values of $\bar{\Lambda}^{SF}$ and λ_1^{SF} extracted from the $b \rightarrow s\gamma$ spectrum by CLEO [4]. Fitting the spectrum to simulated samples with different SF parameters allows us to create a $\Delta\chi^2 = 1$ contour, shown in Figure 2, which we use to estimate theoretical uncertainties. The point with minimum χ^2 corresponds to $\bar{\Lambda}^{SF} = 0.545 \text{ GeV}/c^2$ and $\lambda_1^{SF} = -0.342 \text{ GeV}^2/c^4$.

In the simulation the hadron system X_u is produced with a non-resonant and continuous invariant mass spectrum according to the DFN model. A reweighting of the Fermi motion distribution is used to obtain distributions for different values of $\bar{\Lambda}^{SF}$ and λ_1^{SF} . Finally, the fragmentation of the X_u system into final state hadrons is performed by JETSET [10]. The exclusive charmless semileptonic decays are simulated using the ISGW2 model [11]. The resonant and non-resonant components are combined such that the total branching fraction is consistent with the measured value [1] and that the integrated spectrum agrees with the prediction of Ref. [5]. The resulting m_X distributions for charged and neutral B mesons are shown in Fig. 3. All branching fractions and theory parameters involved in this reweighting are varied within their errors in the evaluation of the associated uncertainty.

While we were writing this paper we became aware of a preliminary interpretation of the $b \rightarrow s\gamma$ energy spectrum measured by Belle [12]. The resulting $\Delta\chi^2 = 1$ contour is shown in Fig. 2: it is consistent with the CLEO one and has smaller uncertainties. A visible shift of the central value of

the measured quantities is expected though because the best fit result from Belle is outside the 1σ CLEO contour. Since there was not enough time to combine the two results, from Belle and CLEO, we prefer to report the results with the CLEO ellipse as primary results and quote the results with the Belle ellipse as a reference for future developments.

2.2 Theoretical Acceptance Estimates

The M_X - q^2 analysis results in the partial branching fraction for charmless semileptonic decays in selected phase space regions. To translate it into a measurement of the total branching fraction, and therefore $|V_{ub}|$, we need the fraction of events inside the measurement region (referred to as “acceptance” in the rest of the paper) as an external input. We choose the results of Bauer, Ligeti and Luke [6] for the acceptance corrections. These authors perform an operator-product-expansion-based calculation which includes $\mathcal{O}(\alpha_s^2)$ and $\mathcal{O}(1/m_b^2)$ corrections in a region of phase space where the non-perturbative effects due to the shape function are small. Their results show that the theoretical uncertainties due to the extrapolation to the full phase space can be significantly reduced with respect to a measurement based on a single M_X cut by moving the M_X cut to the highest practical value allowed by the charm semileptonic background, and by reducing the q^2 cut as low as possible. As a cross-check, acceptances computed with the DFN model presented in the previous section are also used in the M_X - q^2 analysis.

2.3 Simulation of Background Processes

In order to estimate the shape of the background distributions we make use of simulations of $e^+e^- \rightarrow \Upsilon(4S) \rightarrow B\bar{B}$ with the B mesons decaying inclusively. The most relevant backgrounds are due to $\bar{B} \rightarrow X_c \ell \bar{\nu}$ events. The simulation of these processes uses an HQET parametrization of form factors for $\bar{B} \rightarrow D^* \ell \bar{\nu}$ [13], and models for $\bar{B} \rightarrow D^{(*)} \pi \ell \bar{\nu}$ [14], and $\bar{B} \rightarrow D \ell \bar{\nu}, D^{**} \ell \bar{\nu}$ [11].

3 Common Analysis Aspects

The event selection and reconstruction and the measurements of branching fractions follow closely the strategy described in Ref. [1] and represents the common base for the analyses presented here. However, each analysis may differ in some details. This is particularly true for the measurement of exclusive branching fractions. This section describes aspects in common to all studies. Details specific to each analysis are provided in the following sections.

3.1 Event Reconstruction and Selection

In this paper we study the recoil of fully reconstructed B in hadronic decay modes (B_{reco}), which is a moderately pure sample with known flavor and four-momentum. We select B_{reco} decays of the type $B \rightarrow \bar{D}Y$, where D refers to a charm meson, and Y represents a collection of hadrons with a total charge of ± 1 , composed of $n_1\pi^\pm + n_2K^\pm + n_3K_s^0 + n_4\pi^0$, where $n_1 + n_2 < 6$, $n_3 < 3$, and $n_4 < 3$. Using D^- and D^{*-} (\bar{D}^0 and \bar{D}^{*0}) as seeds for B^0 (B^+) decays, we reconstruct about 1000 different decay chains. Overall, we correctly reconstruct one B candidate in 0.3% (0.5%) of the $B^0\bar{B}^0$ (B^+B^-) events. The kinematic consistency of a B_{reco} candidate with a B meson decay is checked using two variables, the beam-energy-substituted mass $m_{ES} = \sqrt{s/4 - \vec{p}_B^2}$ and the energy difference, $\Delta E = E_B - \sqrt{s}/2$. Here \sqrt{s} refers to the total energy in the $\Upsilon(4S)$ center of mass frame,

and \vec{p}_B and E_B denote the momentum and energy of the B_{reco} candidate in the same frame. For signal events the m_{ES} distribution peaks at the B meson mass, while ΔE is consistent with zero. We require $\Delta E = 0$ within approximately three standard deviations.

A semileptonic decay of the other B meson (B_{recoil}) is identified by the presence of a charged lepton with momentum in the B_{recoil} rest frame (p^*) higher than $1 \text{ GeV}/c$. In addition, the detection of missing energy and momentum in the event is taken as evidence for the presence of a neutrino. The hadronic system X is reconstructed from charged tracks and energy depositions in the calorimeter that are not associated with the B_{reco} candidate or the identified lepton. Care is taken to eliminate fake charged tracks, as well as low-energy beam-generated photons and energy depositions in the calorimeter from charged and neutral hadrons. The neutrino four-momentum p_ν is estimated from the missing momentum four-vector $p_{miss} = p_{\Upsilon(4S)} - p_{B_{reco}} - p_X - p_\ell$, where all momenta are measured in the laboratory frame, and $p_{\Upsilon(4S)}$ refers to the $\Upsilon(4S)$ meson.

Undetected particles and measurement uncertainties affect the determination of the four-momenta of the X system and neutrino, and lead to a large leakage of $\bar{B} \rightarrow X_c \ell \bar{\nu}$ background from the high M_X into the low M_X region. To improve the resolution on these four-momenta this analysis exploits the well-known kinematics of the $e^+e^- \rightarrow \Upsilon(4S) \rightarrow B\bar{B}$ process and performs a two-constraint kinematic fit to the whole event.

In the sample of reconstructed B decays two backgrounds need to be considered: the combinatorial background from $B\bar{B}$ and continuum events, due to random association of tracks and neutral clusters, which does not peak in m_{ES} , and the $B\bar{B}$ background whose m_{ES} distribution has the same shape as the signal. After applying all selection criteria, the remaining combinatorial background is subtracted by performing an unbinned likelihood fit to the m_{ES} distribution. In this fit, the combinatorial background originating from $e^+e^- \rightarrow q\bar{q}$ ($q = u, d, s, c$) continuum and $B\bar{B}$ events is described by an empirical threshold function [15], and the signal is described by a modified Gaussian [16] peaked at the B meson mass.

To reject the background in the sample of semileptonic decays we require exactly one charged lepton with $p^* > 1 \text{ GeV}/c$, a total event charge of zero, and a missing mass consistent with zero ($m_{miss}^2 < 0.5 \text{ GeV}^2/c^4$). These criteria partly suppress the dominant $\bar{B} \rightarrow X_c \ell \bar{\nu}$ decays, many of which contain an additional neutrino or an undetected K_L^0 meson. We explicitly veto the $\bar{B}^0 \rightarrow D^{*+} \ell^- \bar{\nu}$ background by searching candidates for such a decay with a partial reconstruction technique, that is only identifying the π_s^+ from the $D^{*+} \rightarrow D^0 \pi_s^+$ decay and the lepton: since the momentum of the π_s^+ is almost collinear with the D^{*+} momentum in the laboratory frame, we can approximate the energy of the D^{*+} as $E_{D^{*+}} \simeq m_{D^{*+}} \cdot E_{\pi_s}/145 \text{ MeV}/c^2$ and estimate the neutrino mass as $m_\nu^2 = (p_B - p_{D^{*+}} - p_\ell)^2$. Events with $m_\nu^2 > -3 \text{ GeV}^2/c^4$ are likely to be background events and are rejected. Finally, we veto events with charged or neutral kaons in the recoil \bar{B} to reduce the peaking background from $\bar{B} \rightarrow X_c \ell \bar{\nu}$ decays. Charged kaons are identified [7] with an efficiency varying between 60% at the highest and almost 100% at the lowest momenta. The pion misidentification rate is about 2%. The $K_S^0 \rightarrow \pi^+ \pi^-$ decays are reconstructed with an efficiency of 80% from pairs of oppositely charged tracks with an invariant mass between 486 and 510 MeV/c^2 .

3.2 Measurement of Charmless Semileptonic Branching Ratios

To reduce the systematic uncertainties in the derivation of branching fractions, the observed number of signal events, corrected for peaking background and efficiency, is normalized to the total number of semileptonic decays $\bar{B} \rightarrow X \ell \bar{\nu}$ in the recoil of the B_{reco} candidates. The number of observed B_{reco} events which contain a charged lepton with $p^* > 1 \text{ GeV}/c$ is denoted as N_{sl}^{meas} . It can be related to the true number of semileptonic decays, N_{sl}^{true} and the remaining peaking background

BG_{sl} , estimated with Monte Carlo simulation, by $N_{sl}^{true} = (N_{sl}^{meas} - BG_{sl}) / \epsilon_l^{sl} \epsilon_t^{sl} = N_{sl} / \epsilon_l^{sl} \epsilon_t^{sl}$. Here ϵ_l^{sl} refers to the efficiency for selecting a lepton from a semileptonic B decay with a momentum above p_{cut} in an event with a reconstructed B with efficiency ϵ_t^{sl} . Figure 4 shows the result of the m_{ES} fit used to determine N_{sl}^{meas} .

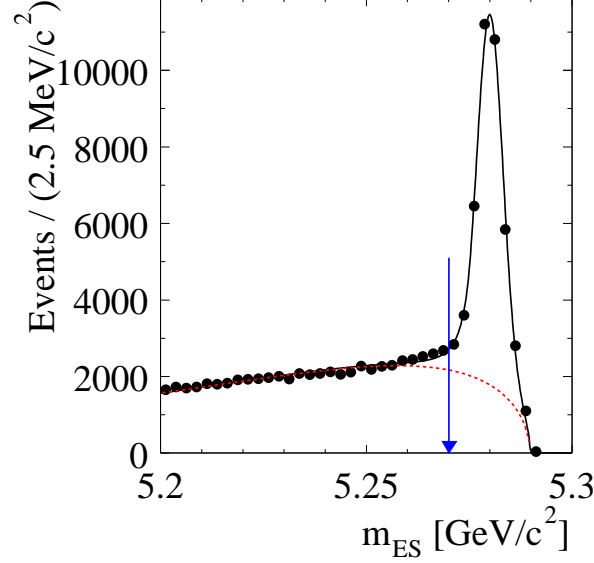


Figure 4: Fit to the m_{ES} distribution for the sample with high momentum lepton.

If we denote as N_u^{meas} the number of events fitted in the sample after all requirements, and with BG_u the peaking background coming from semileptonic decays other than the signal, the true number of signal events N_u^{true} is related to them by

$$N_u = N_u^{meas} - BG_u = \epsilon_{sel}^u \epsilon_l^u \epsilon_t^u N_u^{true}, \quad (2)$$

where the signal efficiency ϵ_{sel}^u accounts for all selection criteria applied on the sample after the requirement of a high momentum lepton.

To measure BG_u in the inclusive studies, the peaking background (BG_u) is estimated by performing a χ^2 fit on the M_X or $M_X - q^2$ distributions, resulting from m_{ES} fits in individual M_X or $M_X - q^2$ bins, with the shape of the background estimated from Monte Carlo simulation, and its normalization free to vary. An example of such a χ^2 fit for the M_X analysis is shown in Fig. 5. For the exclusive analysis the background normalization is taken from Monte Carlo scaled to the data luminosity.

The ratio between the branching fractions for the signal and $\bar{B} \rightarrow X \ell \bar{\nu}$ decays is

$$R_{u/sl} = \frac{\mathcal{B}(\text{signal})}{\mathcal{B}(\bar{B} \rightarrow X \ell \bar{\nu})} = \frac{N_u^{true}}{N_{sl}^{true}} = \frac{(N_u^{meas} - BG_u) / (\epsilon_{sel}^u)}{(N_{sl}^{meas} - BG_{sl})} \times \frac{\epsilon_l^{sl} \epsilon_t^{sl}}{\epsilon_l^u \epsilon_t^u}. \quad (3)$$

The efficiency ratio is expected to be close to, but not equal to unity. Due to the difference in multiplicity and the different lepton momentum spectra, we expect the tag efficiency ϵ_t and lepton efficiency ϵ_l to be slightly different for the two classes of events. The signal branching fraction is

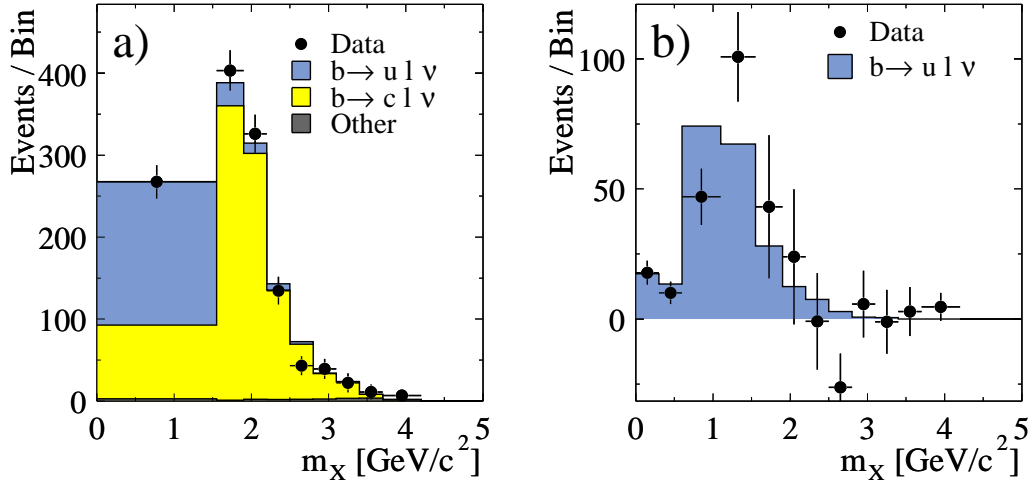


Figure 5: χ^2 fit to the m_X distribution: a) data (points) and fit components, and b) data and signal MC after subtraction of the $b \rightarrow c \ell \nu$ and the “other” backgrounds.

then obtained from $R_{u/sl}$ using the $\bar{B} \rightarrow X_c \ell \bar{\nu}$ branching ratio measured in *BABAR*,

$$\mathcal{B}(\bar{B} \rightarrow X_c \ell \bar{\nu}) = (10.61 \pm 0.16(\text{exp.}) \pm 0.06(\text{theo.}))\% \quad [17]. \quad (4)$$

which, given the previous *BABAR* measurement for the charmless semileptonic branching ratio [1], corresponds to a total semileptonic branching fraction of $\mathcal{B}(\bar{B} \rightarrow X \ell \bar{\nu}) = (10.83 \pm 0.19)\%$.

3.3 Systematic Uncertainties

Most of the systematic uncertainties are common to all analyses. Uncertainties related to the reconstruction of charged tracks are determined by removing randomly a fraction of tracks corresponding to the uncertainty in the track finding efficiency (1.3% for tracks with transverse momentum $p_\perp > 0.2 \text{ GeV}/c$ and 2.5% for tracks with $p_\perp < 0.2 \text{ GeV}/c$). The systematic error due to the reconstruction of neutral particles in the EMC is studied by varying the resolution and efficiency to match those found in control samples in data.

We estimate the systematic error due to particle identification by varying the electron and kaon identification efficiencies by $\pm 2\%$ and the muon identification efficiency by $\pm 3\%$. The misidentification probabilities are varied by 15% for all particles.

The uncertainty of the B_{reco} combinatorial background subtraction is estimated by changing the signal shape function to a Gaussian function instead of the empirical function of Ref. [16]. We evaluated the effect of cross-feed between B^0 and B^+ decays by repeating the analysis with only the $B^0 \bar{B}^0$ or the $B^+ B^-$ Monte Carlo.

The impact of the charm semileptonic branching fractions has been estimated by varying each of the exclusive branching fractions within one standard deviation of the current world average [18]. Similarly, the branching fractions of charm mesons have been varied, both for exclusive decays and for inclusive kaon production. To study the cross-feed among the charmless modes we also varied the number of charmless exclusive semileptonic decays by 30% for $\bar{B} \rightarrow \pi \ell \bar{\nu}$ and $\bar{B} \rightarrow \rho \ell \bar{\nu}$, by 40% for $\bar{B} \rightarrow \omega \ell \bar{\nu}$ and by 100% for the remaining exclusive charmless semileptonic B decays.

In presenting the results the systematic effects are divided into the following categories: uncertainties related to detector and reconstruction simulation (tracking reconstruction, neutral reconstruction, lepton identification, charged Kaon identification), σ_{det} ; uncertainties related to the theoretical model of the non-resonant $b \rightarrow u\ell\bar{\nu}$ decays, σ_{theo} ; uncertainties related to other aspects of the $b \rightarrow u\ell\bar{\nu}$ simulation (resonant signal decay branching fractions, $s\bar{s}$ production, hadronization, etc.), $\sigma_{ul\nu}$; uncertainties due to the limited available Monte Carlo statistics (σ_{MCstat}); uncertainties related to background simulation and subtraction ($\bar{B} \rightarrow D^{(*,**)}\ell\bar{\nu}$ and D branching fractions, fit to the M_X distribution), σ_{bkg} ; uncertainties related to the subtraction of the combinatorial background and cross-feed, σ_{breco} .

4 One-dimensional M_X analysis

We already published a measurement of $|V_{ub}|$ on $\bar{B} \rightarrow X_u\ell\bar{\nu}$ events with $M_X < 1.55 \text{ GeV}/c^2$ [1] and subtracting backgrounds with a one-dimensional fit to the M_X distribution (see Fig. 5). The values for the shape function parameters used were $\bar{\Lambda}^{SF} = 0.48 \pm 0.12 \text{ GeV}$ and $\lambda_1^{SF} = -0.30 \pm 0.11 \text{ GeV}^2$ and a correlation of -80% [9] (see Fig. 2). Since this publication, there have been developments in the theoretical interpretation. Here we report the updated measurement of $|V_{ub}|$ obtained by varying the shape function parameters as stated in Sec. 2.1, the new central value being $\bar{\Lambda}^{SF} = 0.545 \text{ GeV}/c^2$ and $\lambda_1^{SF} = -0.342$. The experimental systematic errors considered are the same and correspond to the sum in quadrature of σ_{det} , $\sigma_{ul\nu}$, σ_{bkg} , σ_{MCstat} , and σ_{breco} . The measured total inclusive branching ratio is

$$R_{u/sl} = 0.0234 \pm 0.0027(\text{stat.}) \pm 0.0026(\text{sys.})^{+0.0064}_{-0.0038}(\text{theo.}) \quad (5)$$

which translates into a total inclusive branching fraction

$$\mathcal{B}(\bar{B} \rightarrow X_u\ell\bar{\nu}) = (2.53 \pm 0.29(\text{stat.}) \pm 0.28(\text{sys.})^{+0.69}_{-0.41}(\text{theo.})) \times 10^{-3}. \quad (6)$$

From the relationship between the inclusive branching fraction and $|V_{ub}|$ (obtained from Eq. 2 in Ref. [4] having updated the OPE parameters to the measurement of *BABAR* [17])

$$|V_{ub}| = 0.00424 \left(\frac{\mathcal{B}(\bar{B} \rightarrow X_u\ell\bar{\nu})}{0.002} \frac{1.604 \text{ ps}}{\tau_B} \right)^{1/2} \times (1.0 \pm 0.048(\text{OPE} + m_b)). \quad (7)$$

Here the average B^0 and B^\pm lifetime is $\tau_B = 1.604 \text{ ps}$ [19]. The “ $\text{OPE} + m_b$ ” uncertainty is due to perturbative and non perturbative corrections, and to the uncertainty on the b -quark mass (m_b). We then obtain

$$|V_{ub}| = (4.77 \pm 0.28(\text{stat.}) \pm 0.28(\text{sys.})^{+0.65}_{-0.39}(\text{theo.}) \pm 0.23(\text{OPE} + m_b))10^{-3}, \quad (8)$$

consistent within the shape function errors with the published $|V_{ub}| = (4.62 \pm 0.28(\text{stat.}) \pm 0.28(\text{sys.}) \pm 0.40(\text{theo.}) \pm 0.26(\text{OPE} + m_b)) \times 10^{-3}$.

5 Unfolding the M_X Spectrum

The observed M_X spectrum is one of the main results of the M_X analysis (see Fig. 5). In order to convert this into a universal observable, we need to unfold detector and selection effects. To increase

sensitivity to the true distribution, the spectrum is re-binned in 310 MeV/ c^2 bins in order to match the resolution. From the measured M_X spectrum, represented by a vector, \vec{x}^{meas} , we extract the unfolded spectrum, \vec{x}^{tru} . The relationship between the two spectra is $\hat{A} \vec{x}^{\text{tru}} = \vec{x}^{\text{meas}}$ [20], where the detector response matrix \hat{A} describes the effects of limited efficiency and finite resolution of the measurement. \hat{A} is estimated on signal MC with the hybrid model described in Sec. 2.1 and with $\bar{\Lambda}^{SF}$ and λ_1^{SF} set to the CLEO best fit values. To reduce systematic uncertainties the simulation has been refined: to account for the unknown details of the fragmentation of quarks into hadrons, we divide the sample into several categories according to the event multiplicity of charged and neutral particles and adjust the fraction of events in each category in MC to match the one observed in data.

In practice, \hat{A} is a non-invertible matrix. Additionally, the uncertainties on the measured spectrum have to be taken into account adequately. We use an unfolding method based on a singular value decomposition of the detector response matrix and a suitable regularization procedure of the unfolded result as described in Ref. [20].

The systematic uncertainties considered are those described in Sec. 3. The systematic effects on the measured spectrum \vec{x}^{meas} are evaluated, each giving rise to a covariance matrix, \hat{C}_k^{meas} , on the measured spectrum. To propagate the covariance matrices for the measured distribution of $M_X(\hat{C}_k^{\text{meas}})$ to covariance matrices on the unfolded spectrum \hat{C}_k^{unf} , two different approaches have been taken depending on whether the response matrix is affected by the systematic under study. In the case of a constant response matrix, e.g. for background modelling, the observed spectrum is smeared a large number of times according to \hat{C}_k^{meas} , the spectra are unfolded and the variations of the result in each bin give rise to \hat{C}_k^{unf} . When the systematics affect the response matrix, e.g. for tracking and neutral efficiencies, the whole measurement is redone with the appropriate changes in reconstruction and the spread serves for the determination of \hat{C}_k^{unf} . The covariance matrix \hat{C}^{unf} is computed as a sum of the individual covariance matrices arising from the different systematic errors, $\hat{C}^{\text{unf}} = \sum_k \hat{C}_k^{\text{unf}}$.

The resulting unfolded spectrum needs to be corrected for a small possible bias arising from the regularization procedure. To estimate this bias we use the unfolded spectrum \vec{x}^{unf} , apply the detector response matrix \hat{A} to it and fluctuate the resulting spectrum using the covariance matrix on the measured spectrum. These spectra are then unfolded and the bin-by-bin mean deviation from the original \vec{x}^{unf} is taken as bias.

5.1 Unfolding results

Figure 6 shows the unfolded spectrum \vec{x}^{unf} normalized to unit area and its cumulative. The errors on the spectrum are given by the square-roots of the diagonal elements of the covariance matrix \hat{C}^{unf} . Detailed listings of \vec{x}^{unf} and \hat{C}^{unf} are given in Table 7 and 8 in Appendix A. The uncertainties on the cumulative distribution take the bin-by-bin correlations of the unfolded spectrum into account. In Fig. 6 we also show a comparison of the data with Monte Carlo samples simulated with SF parameters corresponding to the CLEO best fit and extremes of the $\Delta\chi^2 = 1$ contour. The sensitivity of these spectra to the SF parameters is comparable with the CLEO $b \rightarrow s\gamma$ constraint.

Finally, we compute the first moment $\mathcal{M}_1 = \int_0^{M_{X,0}} M_X f(M_X) dM_X / (\int_0^{M_{X,0}} f(M_X) dM_X)$ and second central moment $\mathcal{M}_2' = \int_0^{M_{X,0}} (M_X - \mathcal{M}_1)^2 f(M_X) dM_X / (\int_0^{M_{X,0}} f(M_X) dM_X)$ from the unfolded spectrum $f(M_X)$, for different upper bounds $M_{X,0}$ on the M_X spectrum. Table 1 shows the measured moments for two different values of $M_{X,0}$: 5 GeV/ c^2 , corresponding to no cut at all, and

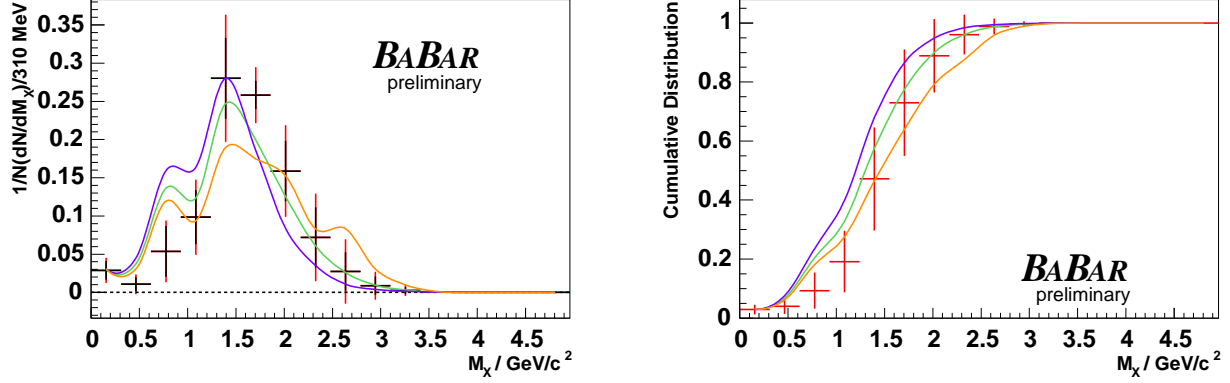


Figure 6: The unfolded spectrum normalized to unit area (left) and its cumulative distribution (right) as a function of M_X . The spectrum and the cumulative distribution from MC with the CLEO best fit $\bar{A}^{SF} = 0.545 \text{ GeV}/c^2$ and $\lambda_1^{SF} = -0.342$ is shown in green (middle). The orange (highest) and violet (lowest) spectra and cumulative distributions correspond to the two extreme points of the CLEO ellipse (see Fig. 2), $\bar{A}^{SF} = 0.800$ and $0.435 \text{ GeV}/c^2$ and to $\lambda_1^{SF} = -1.22$ and -0.16 , respectively. In the left plot black errors are only statistical, while the red ones include always systematics.

$1.86 \text{ GeV}/c^2$. The quoted uncertainties take the bin-by-bin correlations of the unfolded spectrum into account. With a higher precision of the measurement it will be interesting to use moments of the hadronic mass spectrum to constrain the shape function parameters.

Table 1: First and second central moments of the unfolded M_X spectrum. The correlation between the first and second central moment with the same $M_{X,0}$ is also reported. Finally the breakdown of the error into statistical uncertainty ($\sigma_{\text{stat}} \oplus \sigma_{\text{MCstat}}$), uncertainties related to detector effects (σ_{det}), uncertainties related to signal modeling ($\sigma_{\text{ul}\nu} \oplus \sigma_{\text{theo}}$) and to background modeling and subtraction ($\sigma_{\text{bkg}} \oplus \sigma_{\text{breco}}$) is given in GeV/c^2 and GeV^2/c^4 , respectively. The values of \mathcal{M}_1 are in GeV/c^2 while the values of \mathcal{M}_2 are in GeV^2/c^4 .

	$M_{X,0} \text{ (GeV}/c^2\text{)}$	\mathcal{M}	$\sigma(\mathcal{M})$	Correlation	$\sigma_{\text{stat}} \oplus \sigma_{\text{MCstat}}$	σ_{det}	$\sigma_{\text{ul}\nu} \oplus \sigma_{\text{theo}}$	$\sigma_{\text{bkg}} \oplus \sigma_{\text{breco}}$
\mathcal{M}_1	1.86	1.355	0.084		0.064	0.022	0.017	0.023
\mathcal{M}_2	1.86	0.147	0.034	-0.819	0.027	0.010	0.005	0.011
\mathcal{M}_1	5	1.584	0.233		0.166	0.073	0.060	0.101
\mathcal{M}_2	5	0.270	0.099	0.796	0.055	0.037	0.023	0.068

6 Two-dimensional M_X - q^2 analysis

The M_X analysis is systematically limited by the dependence on the shape function. This can be overcome by selecting a phase space region where the shape function effects are small, namely the region at large q^2 values [6]. Therefore we find a trade-off between the statistical and theoretical uncertainties by loosening the M_X cut and applying a q^2 one. Moreover, since most of the theoretical uncertainties are due to the extrapolation from a selected kinematic region to the full phase

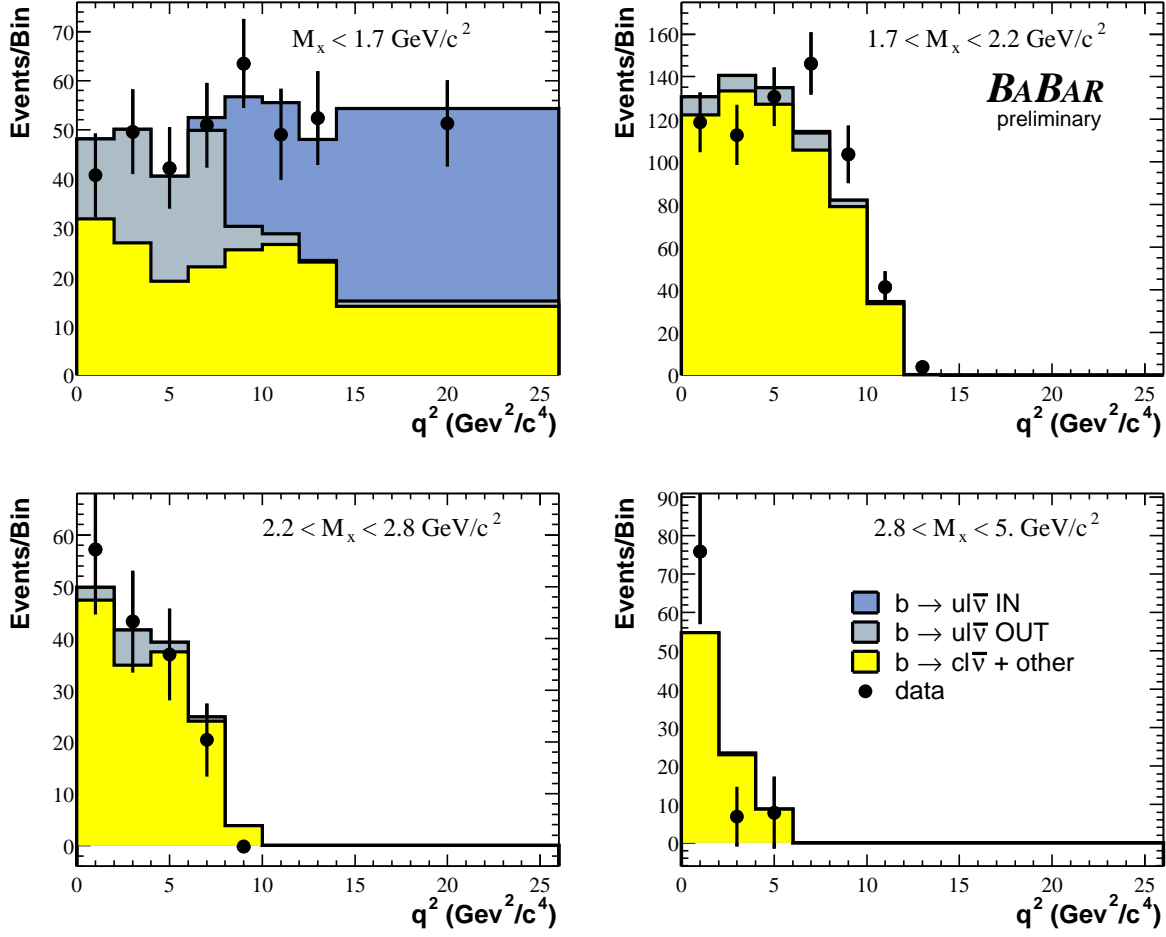


Figure 7: Distributions of q^2 in bins of M_X . Points are data, the blue, light gray and yellow histograms represent the fitted contributions from $b \rightarrow u\ell\bar{\nu}$ events with true $M_X < 1.7 \text{ GeV}/c^2$, $q^2 > 8 \text{ GeV}^2/c^4$, $b \rightarrow u\ell\bar{\nu}$ events not satisfying these requirements, and background events, respectively.

space, measurements of partial branching fractions in different regions of phase space and their extrapolation to the full phase space can serve as tests of the theoretical calculations and models.

In order to extract the partial charmless semileptonic branching ratio in a given region of the M_X - q^2 plane $\Delta\mathcal{B}(\bar{B} \rightarrow X_u\ell\bar{\nu})$, we define as signal the events with true values of the kinematic variables in the chosen region, treating as background those that migrate from outside this region because of the resolution. This means that in applying Eq. 3 we include the $b \rightarrow u\ell\bar{\nu}$ events outside the signal region in BG_u and the quoted efficiencies refer only to events generated in the chosen (M_X - q^2) region. These efficiencies are computed on Monte Carlo, and therefore are based on the DFN model. However, the associated theoretical uncertainty on the final result is small compared to the extrapolation error to the full phase space. We divide the events into two-dimensional bins of M_X and q^2 , we fit the m_{ES} distribution to extract the yield in each bin, and we perform a two-dimensional binned fit of the entire M_X - q^2 distribution in order to extract the signal and background components. The result of the fit is shown in Fig. 7.

Fig. 8a and Table 2 show, for $M_X < 1.7 \text{ GeV}/c^2$, the partial branching fraction $\Delta\mathcal{B}(\bar{B} \rightarrow X_u\ell\bar{\nu})$

as a function of the minimum q^2 cut.

We convert the measured $\Delta\mathcal{B}(\bar{B} \rightarrow X_u \ell \bar{\nu})$ into $|V_{ub}|$ by

$$|V_{ub}| = \sqrt{\frac{192\pi^3}{\tau_B G_F^2 m_b^5} \frac{\Delta\mathcal{B}(\bar{B} \rightarrow X_u \ell \bar{\nu})}{G}} \quad (9)$$

where $\tau_B = 1.61\text{ps}$ and G is a theoretical parameter calculated in the BLL approach [6]. The first factor under the square root is $192\pi^3/(\tau_B G_F^2 m_b^5) = 0.00779$. The measured $|V_{ub}|$ as a function of the q^2 cut is shown in Fig. 8b for the acceptances computed by BLL and by DFN. Note that, since the operator product expansion breaks down when going to low q^2 , the BLL calculation is only possible for higher values of q^2 .

The error on the acceptance as computed by BLL increases for tighter cuts on q^2 . For smaller values of q^2 , the shape function effects increase. In the signal region $q^2 > 8\text{ GeV}^2/c^4$, $M_X < 1.7\text{ GeV}/c^2$ we obtain:

$$\Delta\mathcal{B}(\bar{B} \rightarrow X_u \ell \bar{\nu}, M_X < 1.7\text{ GeV}/c^2, q^2 > 8\text{ GeV}^2/c^4) = (0.88 \pm 0.14(\text{stat.}) \pm 0.13(\text{sys.}) \pm 0.02(\text{theo.})) \times 10^{-3}. \quad (10)$$

To extract $|V_{ub}|$, we take G as computed by BLL and rescale it to the b -quark mass as measured by BABAR[17], obtaining $G = 0.282 \pm 0.053$, corresponding to an acceptance $\epsilon_{BLL} = 0.325 \pm 0.061$. Eq. 9 yields

$$|V_{ub}| = (4.92 \pm 0.39(\text{stat.}) \pm 0.36(\text{sys.}) \pm 0.46(\text{theo.})) \times 10^{-3}. \quad (11)$$

In the DFN model the calculated acceptance is $\epsilon = 0.337_{-0.074}^{+0.037}$ and by using Equation 7 we obtain $|V_{ub}| = (4.85 \pm 0.39(\text{stat.}) \pm 0.36(\text{sys.}) \pm 0.54_{-0.29}^{+0.54}(\text{theo.})) \times 10^{-3}$, in agreement with the extraction based on BLL, as well as with the result from the one-dimensional M_X fit. Figure 8 shows the measured values for $|V_{ub}|$ as a function of the q^2 cut for $M_X < 1.7\text{ GeV}/c^2$, showing good consistency between the different cuts and theoretical framework. Checks were done also with a looser ($M_X < 1.86\text{ GeV}/c^2$) and a tighter ($M_X < 1.5\text{ GeV}/c^2$) cut on M_X , and they give consistent results.

Table 2: Partial branching fraction measurements (in 10^{-3} units) for $M_X < 1.7\text{ GeV}/c^2$ and $q^2 > q_{cut}^2$, as a function of q_{cut}^2 . The different sources of uncertainty (as described in 3.3) are also reported.

$q_{cut}^2 >$	$\Delta\mathcal{B}(\bar{B} \rightarrow X_u \ell \bar{\nu})$	σ_{stat}	σ_{det}	σ_{breco}	σ_{bkg}	σ_{theo}	$\sigma_{ul\nu}$	σ_{MCstat}
0	1.68	0.22	0.15	0.08	0.12	-0.045 +0.035	0.137	0.08
2	1.52	0.20	0.16	0.07	0.11	-0.028 +0.036	0.110	0.07
4	1.33	0.18	0.11	0.06	0.10	-0.040 +0.026	0.116	0.06
6	1.10	0.16	0.14	0.05	0.08	-0.022 +0.018	0.083	0.05
8	0.88	0.14	0.09	0.04	0.06	-0.028 +0.009	0.053	0.05
10	0.55	0.11	0.03	0.02	0.04	-0.006 +0.019	0.027	0.03
12	0.41	0.09	0.04	0.02	0.03	-0.010 +0.000	0.033	0.03
14	0.21	0.06	0.01	0.01	0.02	-0.012 +0.012	0.018	0.02

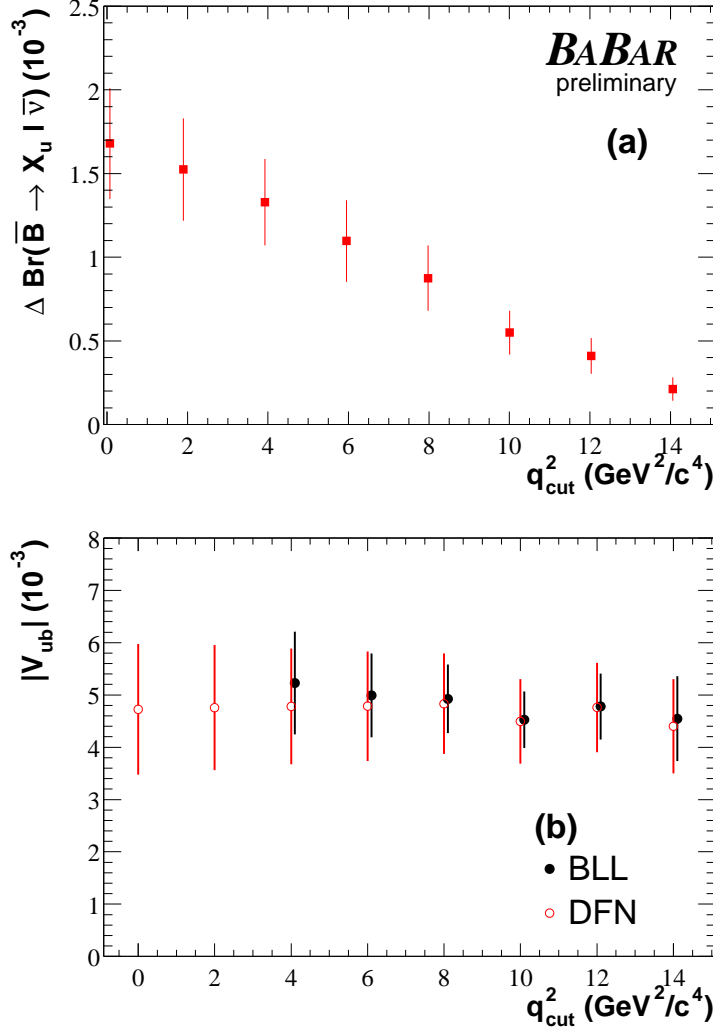


Figure 8: (a) Measured partial branching ratio for $M_X < 1.7 \text{ GeV}/c^2$ and $q^2 > q^2_{\text{cut}}$, as a function of q^2_{cut} . The error bar is the sum in quadrature of statistical, systematical and theoretical uncertainties. (b) Measured value of $|V_{ub}|$ for $M_X < 1.7 \text{ GeV}/c^2$ as a function of the q^2 cut applied when using acceptances from DFN (open points) and BLL (solid points). The error bars include the statistical, systematic and theoretical uncertainties, added in quadrature.

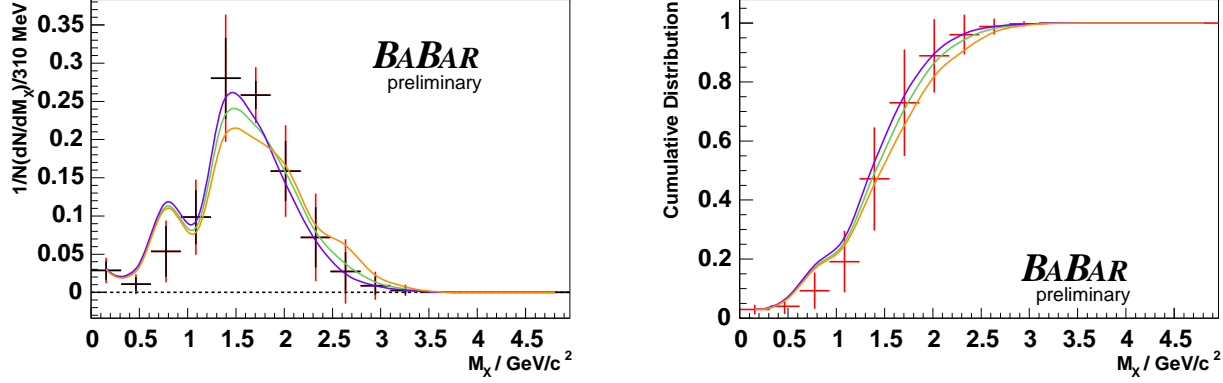


Figure 9: The unfolded spectrum (left) and its cumulative distribution (right) as a function of M_X . The spectrum and the cumulative distribution from MC with the Belle best fit $\bar{A}^{SF} = 0.66 \text{ GeV}/c^2$ and $\lambda_1^{SF} = -0.4 \text{ GeV}^2/c^4$ is shown in green. The orange and violet spectra and cumulative distributions correspond to the two extreme points in the Belle ellipse (see Fig. 2), $\bar{A}^{SF} = 0.600 \text{ GeV}/c^2$ and $\bar{A}^{SF} = 0.748 \text{ GeV}/c^2$ and to $\lambda_1^{SF} = -0.66 (\text{GeV}/c^2)^2$ and $\lambda_1^{SF} = -0.28 (\text{GeV}/c^2)^2$, respectively. In the left plot black errors are only statistical, while the red ones always include systematics.

7 Results based on Belle's estimate of the SF parameters

We report here the results obtained with the SF parameters as estimated from the $b \rightarrow s\gamma$ photon energy spectrum measured by Belle (see Sec. 2.1) and we reinterpret our results by using them in the M_X and M_X - q^2 analyses. The acceptance obtained for the DFN model is lower, and therefore the charmless semileptonic branching fraction and $|V_{ub}|$ are higher. The theoretical systematics due to the shape function parameters is reduced, due to the significantly better precision.

For the M_X analysis we get

$$R_{u/sl} = (2.81 \pm 0.32(\text{stat.}) \pm 0.31(\text{sys.})_{-0.21}^{+0.23}(\text{theo.})) \times 10^{-2} \quad (12)$$

which translates into

$$|V_{ub}| = (5.22 \pm 0.30(\text{stat.}) \pm 0.31(\text{sys.})_{-0.20}^{+0.22}(\text{SF}) \pm 0.25(\text{pert} + 1/\text{mb}^3))10^{-3}. \quad (13)$$

As far as the unfolding is concerned, Fig. 9 compares the measured spectra with the distributions corresponding to the SF parameters measured by Belle.

The partial branching fraction measurements as a function of the q^2 cut obtained by the M_X - q^2 analysis are reported, for $M_X < 1.7 \text{ GeV}/c^2$, in Table 3.

The measurement of the partial branching fraction $\mathcal{B}(\bar{B} \rightarrow X_u \ell \bar{\nu})$ in the region limited by $M_X < 1.7 \text{ GeV}/c^2$, $q^2 > 8 (\text{GeV}/c^2)^2$ is

$$\Delta \mathcal{B}(\bar{B} \rightarrow X_u \ell \bar{\nu}, M_X < 1.7 \text{ GeV}/c^2, q^2 > 8 \text{ GeV}^2/c^4) = (0.90 \pm 0.14(\text{stat.}) \pm 0.14(\text{sys.})_{-0.02}^{+0.01}(\text{theo.})) \times 10^{-3}.$$

By using $G = 0.282 \pm 0.053$ from BLL, we get

$$|V_{ub}| = (4.98 \pm 0.40(\text{stat.}) \pm 0.39(\text{syst.}) \pm 0.47(\text{theo.})) \times 10^{-3}.$$

The DFN acceptance computed at $M_X < 1.7 \text{ GeV}/c^2$ and $q^2 > 8 \text{ (GeV}/c^2)^2$ with the Belle SF parameters is $\epsilon = 0.300^{+0.023}_{-0.028}$. This gives in the DFN framework $|V_{ub}| = (5.18 \pm 0.41_{\text{stat}} \pm 0.40_{\text{syst}}^{+0.25}_{-0.20} \text{ theo}) \times 10^{-3}$.

Figure 10 shows the results for $|V_{ub}|$ as a function of the q^2 cut for $M_X < 1.7 \text{ GeV}/c^2$, for both DFN and BLL. The two models are still consistent within the present accuracies. The stability of the result and the agreement between the two methods seems to indicate that OPE is still valid in this q^2 range.

8 Measurement of Exclusive Charmless Semileptonic Branching Fractions

8.1 Reconstruction of Exclusive Modes.

The reconstruction and selection of the events follows closely the one described in Sec. 3. Hadrons are reconstructed in the following modes:

- π^0 candidates are defined as pairs of photons with an energy in the laboratory $E_\gamma > 30 \text{ MeV}$. In order to further reject combinatorial background we apply a cut on the energy of the more energetic photon in the recoiling B meson rest frame at $E_\gamma^* > 300 \text{ MeV}$.
- ρ^0 candidates are reconstructed using pairs of charged tracks with opposite charge assuming the pion mass. A cut on the momentum of the pions in the recoiling B meson rest frame is applied. The tracks are ordered depending on their momentum and we apply a cut on the more energetic track at $p_\pi^* > 350 \text{ MeV}/c$ and on the other one at $p_\pi^* > 150 \text{ MeV}/c$.
- ρ^+ candidates are reconstructed using one charged track (with opposite charge with respect to the most energetic lepton in the recoil) and one π^0 . We apply a cut on the momentum of the π^0 momentum at $p_{\pi^0}^* > 150 \text{ MeV}/c$.

Table 3: BELLE ellipse: Partial branching fraction $\Delta\mathcal{B}(\bar{B} \rightarrow X_u \ell \bar{\nu})$ measurements (in 10^{-3} units) for different q^2 cuts. M_X is required to be less than $1.7 \text{ GeV}/c^2$. The different sources of uncertainties are also reported.

$q_{\text{cut}}^2 >$	$\Delta\mathcal{B}(\bar{B} \rightarrow X_u \ell \bar{\nu})$	σ_{stat}	σ_{det}	σ_{breco}	σ_{bkg}	σ_{theo}	$\sigma_{\text{ul}\nu}$	σ_{MCstat}
0	1.740	0.231	0.159	0.078	0.129	-0.042 +0.026	0.158	0.078
2	1.584	0.205	0.165	0.071	0.117	-0.037 +0.027	0.145	0.068
4	1.381	0.186	0.113	0.062	0.102	-0.036 +0.026	0.140	0.061
6	1.135	0.161	0.144	0.051	0.084	-0.025 +0.017	0.105	0.053
8	0.896	0.143	0.091	0.040	0.066	-0.017 +0.012	0.064	0.047
10	0.566	0.113	0.026	0.025	0.042	-0.006 +0.013	0.041	0.036
12	0.406	0.085	0.038	0.018	0.030	-0.002 +0.003	0.034	0.026
14	0.207	0.059	0.014	0.009	0.015	-0.007 +0.002	0.026	0.019

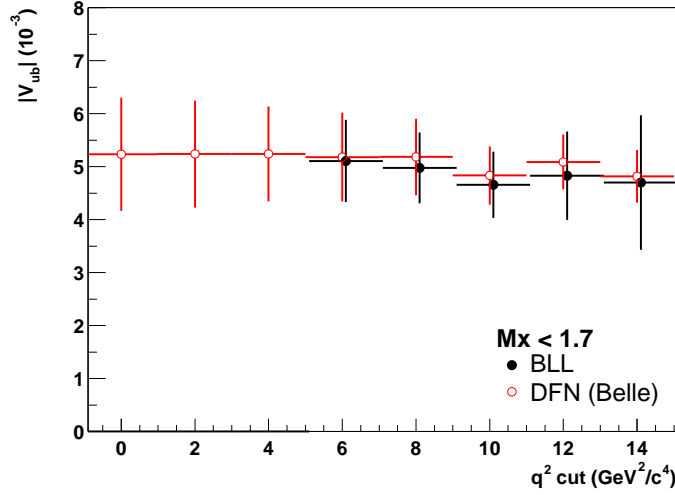


Figure 10: BELLE ellipse: Values for $|V_{ub}|$ as a function of the q^2 cut for $M_X < 1.7 \text{ GeV}/c^2$ by taking acceptances from Bauer, Ligeti and Luke (points) and De Fazio-Neubert (squares). The error is the sum in quadrature of the statistical, systematic and theoretical uncertainties.

- ω candidates are reconstructed in the mode $\omega \rightarrow \pi^+\pi^-\pi^0$ ($\mathcal{B}(\omega \rightarrow \pi^+\pi^-\pi^0) = 89.1\%$) by using pairs of charged tracks with opposite charge and one π^0 . In order to further reject combinatorics we apply a cut rejecting combinations that are at the edge of the Dalitz plot of the three pions.
- η candidates are reconstructed in three decay modes: $\eta \rightarrow \gamma\gamma$ ($BF = 39.4\%$), $\eta \rightarrow \pi^+\pi^-\pi^0$ ($BF = 22.6\%$) and $\eta \rightarrow \pi^0\pi^0\pi^0$ ($BF = 32.5\%$).
- η' candidates are reconstructed in two decay modes: $\eta' \rightarrow \rho\gamma$ ($BF = 29.5\%$) and $\eta' \rightarrow \eta\pi^+\pi^-$ ($BF = 44.3\%$). We apply cuts on the mass of the daughters at $0.508 \text{ GeV}/c^2 < M_\eta < 0.588 \text{ GeV}/c^2$ and $0.625 \text{ GeV}/c^2 < M_{\rho^0} < 0.925 \text{ GeV}/c^2$.
- a_0^0 and a_0^+ candidates are reconstructed in the $\eta\pi^0$ mode. η 's are required to have a reconstructed mass within the range $0.518 \text{ GeV}/c^2 < M_\eta < 0.578 \text{ GeV}/c^2$. We assume a Breit-Wigner width of $71 \pm 7 \text{ MeV}/c^2$ [21] for both a_0^0 and a_0^+ .

In addition to these criteria we also select mass windows around the nominal meson masses as detailed in Table 4

8.2 Event based cuts

The event variables used to reject background are the same as described in Sec. 3, but the cut values are different and have been optimized mode by mode. Also, the missing mass squared (m_{miss}^2) is computed from the lepton and just the charged tracks and photon candidates that form one of the specific hadronic final states we are looking for. This means that if more than one mode is reconstructed in a given event, more than one value of m_{miss}^2 is calculated. For each decay mode the best candidate in an event is chosen on the basis of the χ^2 built from the reconstructed invariant mass of the resonance daughter and m_{miss}^2 . In addition we have applied discriminating variables:

the total photon energy ($E_{neutral}$), the invariant mass of the lepton and the charged track (m_{trk}), the number of reconstructed π^0 and charged tracks in the recoil. A summary of selection criteria per mode is shown in Table 4.

Table 4: Summary of event based cuts and efficiency for all modes. The calculation of the efficiency does not include hadronic B reconstruction efficiency (ϵ_t).

Common cuts	$p^* > 1.0 \text{ GeV}/c$, $N_{lepton} = 1$, $Q_{b(recoil)}Q_\ell > 0$, $Q_{tot} = 0$, $N_K = 0$, no additional charged track in the recoil		
	$\bar{B}^0 \rightarrow \pi^+ \ell \bar{\nu}$	$B^- \rightarrow \pi^0 \ell \bar{\nu}$	$\bar{B}^0 \rightarrow \rho^+ \ell \bar{\nu}$
$m_{miss}^2 \text{ (GeV}^2/c^4)$	$ m_{miss}^2(\pi^+) < 0.3$	$-0.5 < m_{miss}^2(\pi^0) < 0.7$	$ m_{miss}^2(\rho^+) < 0.4$
Mass (GeV/ c^2)	-	$0.11 < m < 0.16$	$0.55 < m < 1.0$
Specific cuts	$E_{neutral} < 0.25 \text{ GeV}$ $ m_{trk} - 3.1 < 0.02 \text{ GeV}/c^2$	-	-
Final eff. ($\epsilon_{sel}\epsilon_l$)	0.302 ± 0.005	0.263 ± 0.007	0.154 ± 0.004
	$B^- \rightarrow \rho^0 \ell \bar{\nu}$	$B^- \rightarrow \omega \ell \bar{\nu}$	$B^- \rightarrow \eta \ell \bar{\nu}$
$m_{miss}^2 \text{ (GeV}^2/c^4)$	$ m_{miss}^2(\rho^0) < 0.4$	$ m_{miss}^2(\omega) < 0.4$	$ m_{miss}^2(\eta) < 0.5$
Mass (GeV/ c^2)	$0.6 < m < 1.0$	$0.74 < m < 0.82$	$0.515 < m < 0.575$
Specific cuts	$N(\pi^0) < 2$ $m_{miss}^2(\omega) < -0.4 \text{ GeV}^2/c^4$	$N(\pi^0) < 6$	$m_{miss}^2(\pi^0) < -1.5 \text{ GeV}^2/c^4$
Final eff. ($\epsilon_{sel}\epsilon_l$)	0.214 ± 0.006	0.109 ± 0.004	0.133 ± 0.006
	$B^- \rightarrow \eta' \ell \bar{\nu}$	$B^- \rightarrow a_0^0 \ell \bar{\nu}$	$\bar{B}^0 \rightarrow a_0^+ \ell \bar{\nu}$
$m_{miss}^2 \text{ (GeV}^2/c^4)$	$ m_{miss}^2(\eta') < 0.5$	$ m_{miss}^2(a_0^0) < 0.5$	$ m_{miss}^2(a_0^+) < 0.5$
Mass (GeV/ c^2)	$0.92 < m < 0.99$	$0.92 < m < 1.04$	$0.92 < m < 1.04$
Specific cuts		$m_{miss}^2(\omega) > 1.5 \text{ GeV}^2/c^4$ $m_{miss}^2(\eta) > 0.5 \text{ GeV}^2/c^4$	$m_{miss}^2(\rho^+) > 1.0 \text{ GeV}^2/c^4$
Final eff. ($\epsilon_{sel}\epsilon_l$)	0.066 ± 0.004	0.049 ± 0.008	0.074 ± 0.007

8.3 Systematic Uncertainties

The systematics are summarized in Table 5. The sources common to the other analyses are described in Sec. 3, but there are also sources of systematic uncertainty which are specific to this exclusive analysis.

We evaluate the impact of different form factor calculations changing the ISGW2 model (our default) to light cone sum rule calculations by reweighting events. This error is included in σ_{ulv} .

The systematic effect due to the non-resonant structure has been evaluated by using a different mixture that allows the non-resonant contribution to go down to 2π masses (the same model used in the inclusive analysis [1]). The $B^- \rightarrow \rho^0 \ell \bar{\nu}$ channel has a different treatment since the $\pi^+\pi^-$ non-resonant contamination may not be negligible and it cannot be distinguished from the signal component. In order to quantify the non-resonant contribution we use an approach that is very similar to the one described in [22]. From measurements of e^+e^- data and τ decays and from Bose symmetry considerations the non-resonant contribution has to come from the isospin $I = 0$

component. The isospin relationships therefore predict no non-resonant component in $\bar{B}^0 \rightarrow \rho^+ \ell \bar{\nu}$, and a ratio 2:1 between the non resonant contribution due to $B^- \rightarrow \pi^0 \pi^0 \ell \bar{\nu}$ and $B^- \rightarrow \pi^+ \pi^- \ell \bar{\nu}$. By measuring the $B^- \rightarrow \pi^0 \pi^0 \ell \bar{\nu}$ from our data we obtain

$$\mathcal{B}(B^- \rightarrow \pi^0 \pi^0 \ell \bar{\nu}) < 0.6 \times 10^{-4} \quad (90 \% \text{ C.L.}) \quad (14)$$

in the mass region $0.6 \text{ GeV}/c^2 < m(\pi^0 \pi^0) < 1.0 \text{ GeV}/c^2$. The 68% C.L. upper limit is used to evaluate the systematic uncertainty due to the non-resonant component. In the following we will quote $\mathcal{B}(B^- \rightarrow \text{“}\rho^0\text{”} \ell \bar{\nu})$, assuming no non-resonant contribution since we measured a rate for $B^- \rightarrow \pi^0 \pi^0 \ell \bar{\nu}$ which is compatible with zero. On the other hand this systematic uncertainty is taken into account in the combination of the $\bar{B}^0 \rightarrow \rho^+ \ell \bar{\nu}$, $B^- \rightarrow \rho^0 \ell \bar{\nu}$ and $B^- \rightarrow \omega \ell \bar{\nu}$ results where isospin and quark model relations are used (see next section). This component is included in σ_{bkg} .

Table 5: Summary of the systematic uncertainties in the measurement of the $R_{u/sl}$ defined in Eq. 3.

	Uncertainty on $R_{u/sl} [\times 10^{-4}]$				
	$\bar{B}^0 \rightarrow \pi^+ \ell \bar{\nu}$	$B^- \rightarrow \pi^0 \ell \bar{\nu}$	$\bar{B}^0 \rightarrow \rho^+ \ell \bar{\nu}$	$B^- \rightarrow \text{“}\rho^0\text{”} \ell \bar{\nu}$	$B^- \rightarrow \omega \ell \bar{\nu}$
$R_{u/sl} [\times 10^{-4}]$	0.86	0.81	3.3	0.92	1.12
σ_{stat}	0.33	0.25	1.1	0.34	0.49
σ_{det}	0.015	0.063	0.250	0.026	0.076
σ_{breco}	0.090	0.050	0.257	0.071	0.074
σ_{bkg}	0.043	0.046	0.475	0.047	0.064
σ_{ulv}	0.029	0.028	0.234	0.059	0.078
σ_{MCstat}	0.048	0.065	0.257	0.092	0.146
Total syst. error	0.115	0.117	0.652	0.141	0.207
	$B^- \rightarrow \eta \ell \bar{\nu}$	$B^- \rightarrow \eta' \ell \bar{\nu}$	$B^- \rightarrow a_0^0 \ell \bar{\nu}$	$\bar{B}^0 \rightarrow a_0^+ \ell \bar{\nu}$	
$R_{u/sl} [\times 10^{-4}]$	0.34	2.4	1.8	0.5	
σ_{stat}	0.36	1.0	1.0	1.3	
σ_{det}	0.167	0.199	0.754	0.081	
σ_{breco}	0.046	0.122	0.106	0.133	
σ_{bkg}	0.038	0.106	0.072	0.047	
σ_{ulv}	0.004	0.034	0.180	0.050	
σ_{MCstat}	0.073	0.290	0.293	0.204	
Total syst. error	0.192	0.389	0.839	0.266	

8.4 Results of the exclusive measurements.

For the extraction of the ratio of branching ratios we use Equation 3. The only difference is in the inclusive semileptonic branching ratios since we use $\mathcal{B}(\bar{B}^0 \rightarrow X \ell \bar{\nu}) = (10.4 \pm 0.3)\%$ and $\mathcal{B}(B^- \rightarrow X \ell \bar{\nu}) = (11.3 \pm 0.3)\%$, obtained from the inclusive semileptonic branching ratio [17] and the lifetime ratio between neutral and charged B mesons [18]. The results are summarized in Table 6. In Figs. 11-19 the projections of the result on the reconstructed mass and on the m_{miss}^2 variable are shown for each mode. All selection criteria are applied except for the ones on the variable that is plotted.

Table 6: Fit results for all modes.

	N_{excl}^{meas}	BG_{excl}	ϵ_{sel}^{excl}	$N_{sl}^{meas} - BG_{sl}$	$\frac{\epsilon_l^{sl}}{\epsilon_l^{excl}}$	$R_{u/sl} [\times 10^{-3}]$
$\bar{B}^0 \rightarrow \pi^+ \ell \bar{\nu}$	11.1 ± 3.9	0.9 ± 0.5	0.65 ± 0.03	15350 ± 200	0.84 ± 0.01	$0.86 \pm 0.33(\text{stat})$
$B^- \rightarrow \pi^0 \ell \bar{\nu}$	15.5 ± 4.1	2.3 ± 1.2	0.56 ± 0.03	25250 ± 300	0.87 ± 0.01	$0.81 \pm 0.25(\text{stat})$
$\bar{B}^0 \rightarrow \rho^+ \ell \bar{\nu}$	20.1 ± 5.7	2.4 ± 1.7	0.31 ± 0.02	13100 ± 200	0.76 ± 0.01	$3.3 \pm 1.1(\text{stat})$
$B^- \rightarrow \text{"}\rho^0\text{"} \ell \bar{\nu}$	15.7 ± 4.3	4.0 ± 1.0	0.45 ± 0.03	22500 ± 200	0.79 ± 0.01	$0.92 \pm 0.34(\text{stat})$
$B^- \rightarrow \omega \ell \bar{\nu}$	9.3 ± 3.3	1.7 ± 0.8	0.21 ± 0.02	25250 ± 300	0.77 ± 0.01	$1.12 \pm 0.49(\text{stat})$
$B^- \rightarrow \eta \ell \bar{\nu}$	3.8 ± 2.7	1.3 ± 0.6	0.28 ± 0.01	23050 ± 200	0.87 ± 0.02	$0.34 \pm 0.36(\text{stat})$
$B^- \rightarrow \eta' \ell \bar{\nu}$	13.9 ± 4.2	4.3 ± 1.2	0.14 ± 0.01	23050 ± 200	0.87 ± 0.02	$2.4 \pm 1.0(\text{stat})$
$B^- \rightarrow a_0^0 \ell \bar{\nu}$	9.1 ± 3.5	2.5 ± 0.9	0.11 ± 0.01	23050 ± 200	0.91 ± 0.03	$2.4 \pm 1.3(\text{stat})$
$\bar{B}^0 \rightarrow a_0^+ \ell \bar{\nu}$	3.0 ± 3.5	1.4 ± 0.9	0.16 ± 0.02	14700 ± 200	0.87 ± 0.03	$0.6 \pm 1.4(\text{stat})$

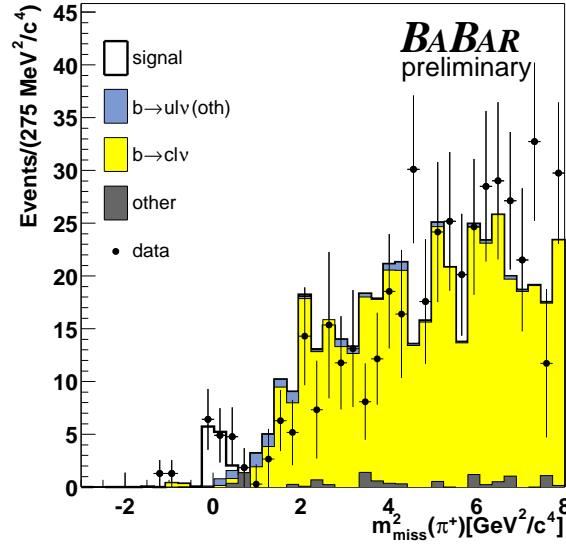


Figure 11: $\bar{B}^0 \rightarrow \pi^+ \ell \bar{\nu}$: Projection of the fit result onto the m_{miss}^2 variable.

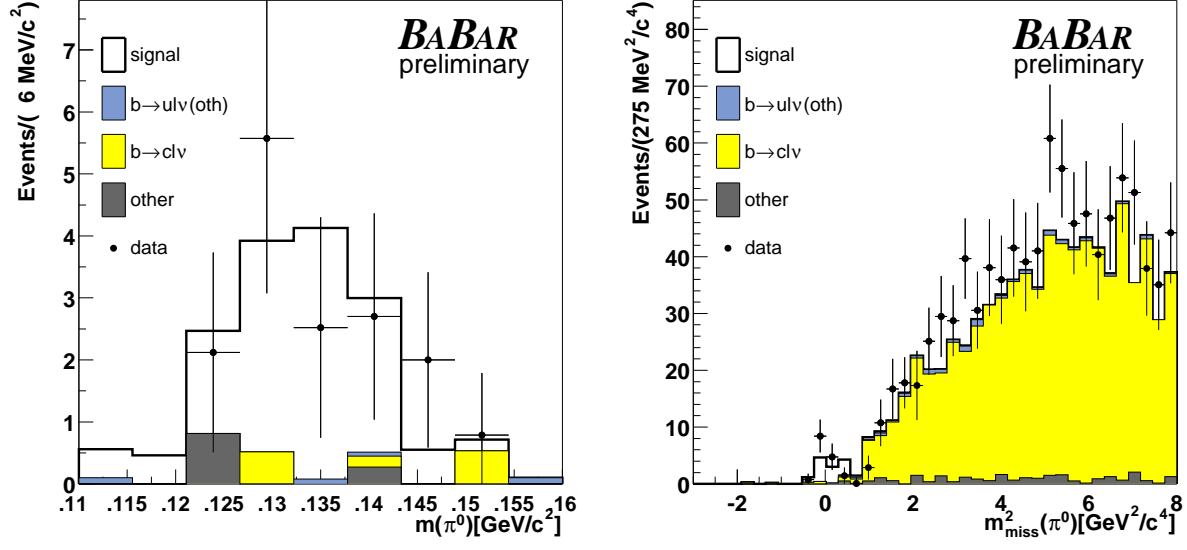


Figure 12: $B^- \rightarrow \pi^0 \ell \bar{\nu}$: Projection of the fit result onto the $m(\pi^0)$ (left) and m_{miss}^2 (right) variables.

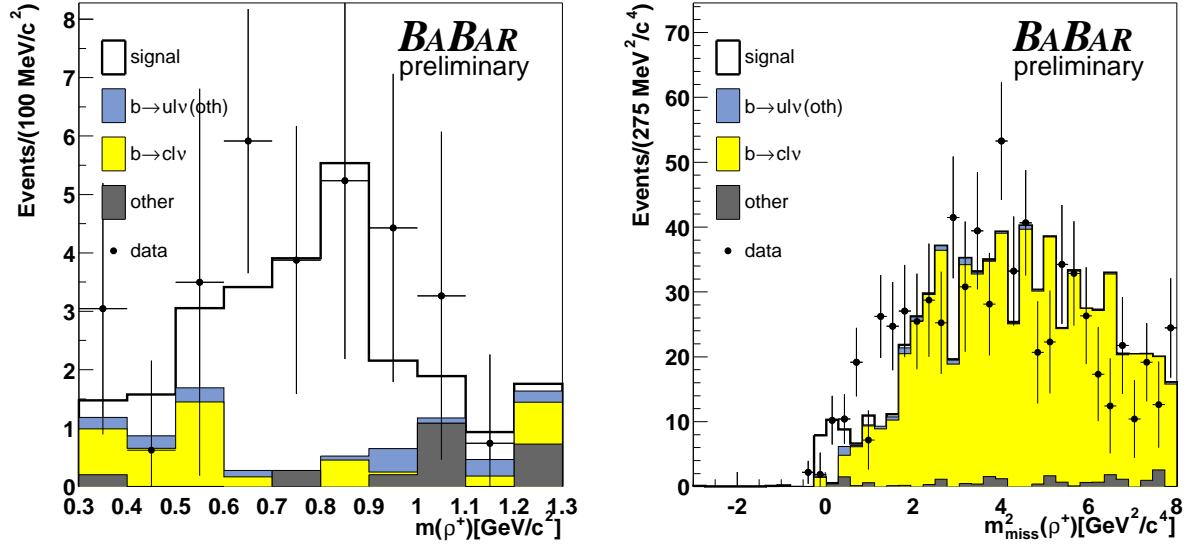


Figure 13: $\bar{B}^0 \rightarrow \rho^+ \ell \bar{\nu}$: Projection of the fit result onto the $m(\rho^+)$ (left) and m_{miss}^2 (right) variables.

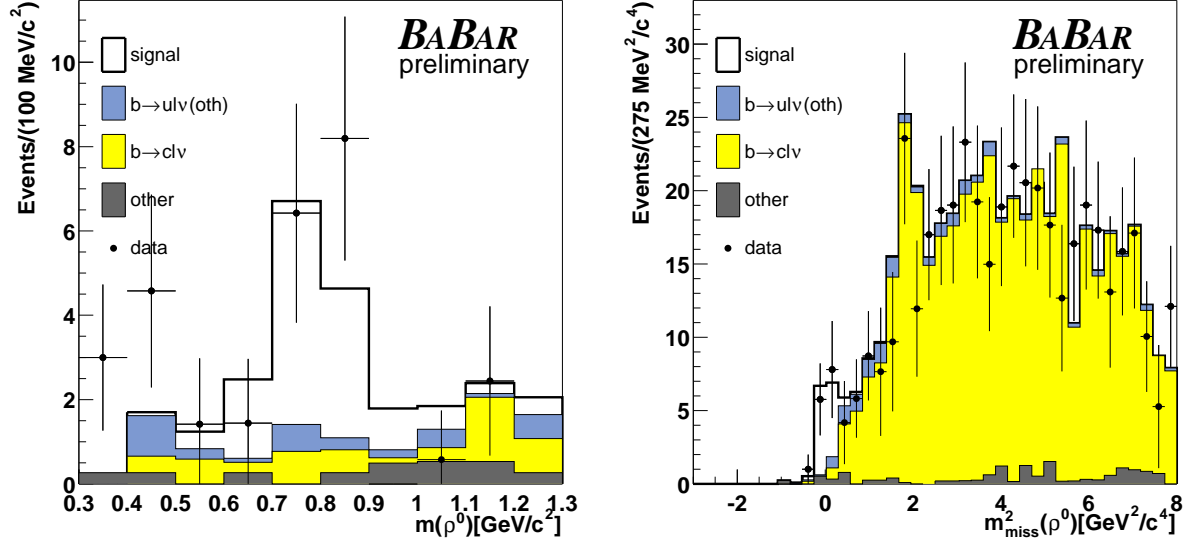


Figure 14: $B^- \rightarrow \rho^0 \ell \bar{\nu}$: Projection of the fit result onto the $m(\pi^+\pi^-)$ (left) and m_{miss}^2 (right) variables. Here “ ρ^0 ” means that no $B^- \rightarrow \pi^+\pi^-\ell\bar{\nu}$ non-resonant contribution is taken into account.

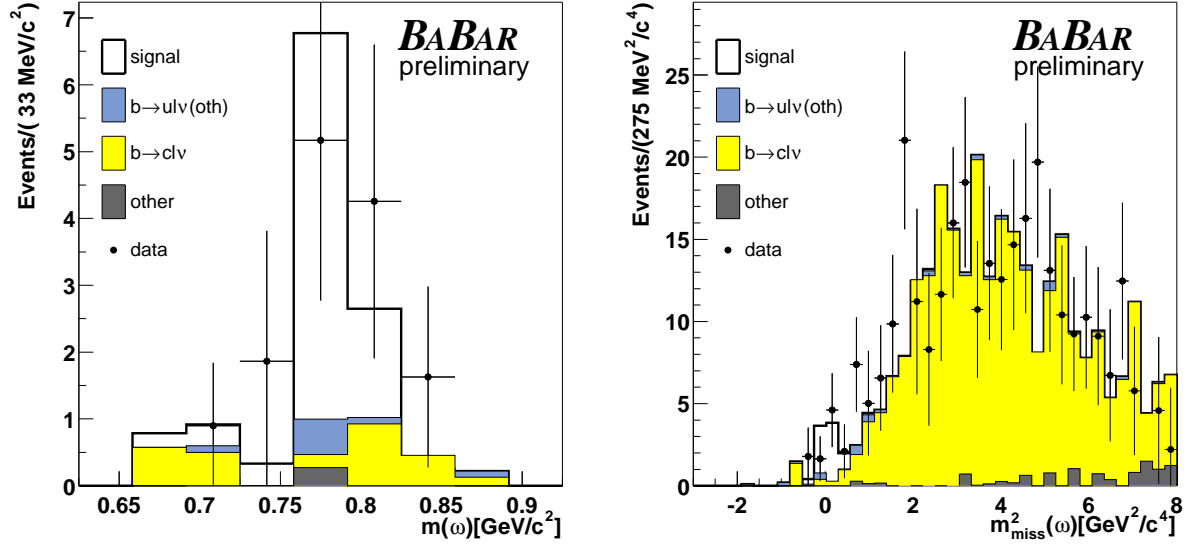


Figure 15: $B^- \rightarrow \omega \ell \bar{\nu}$: Projection of the fit result onto the $m(\omega)$ (left) and m_{miss}^2 (right) variables.

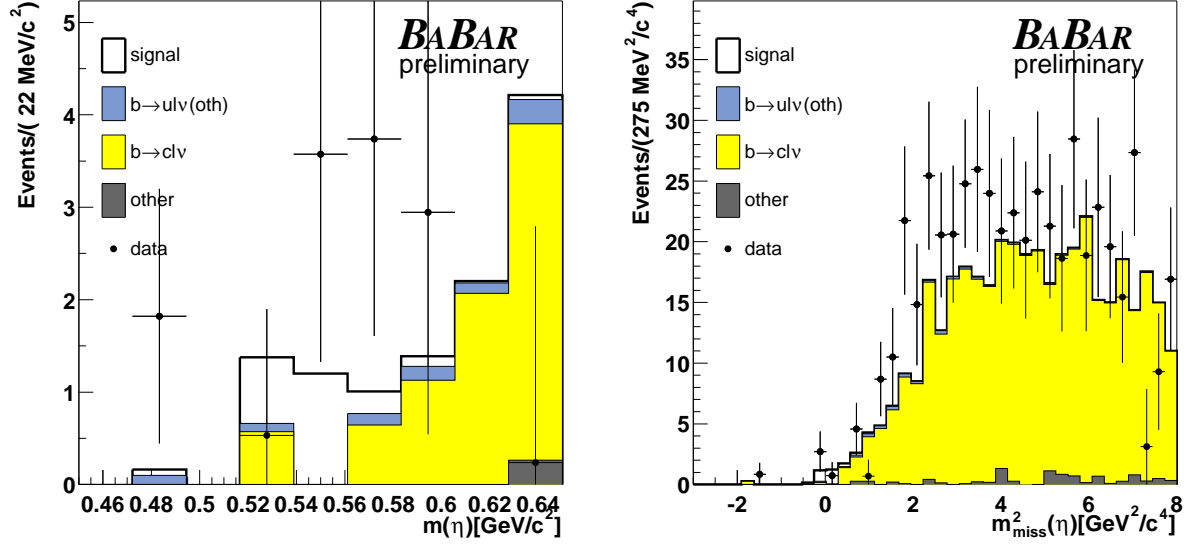


Figure 16: $B^- \rightarrow \eta \ell \bar{\nu}$: Projection of the fit result onto the $m(\eta)$ (left) and $m_{miss}^2(\eta)$ (right) variables.

Since the branching ratios of the a_0^0 , a_0^+ decays are not known, the results for these channels will include the $a_0^0 \rightarrow \eta \pi^0$ and $a_0^+ \rightarrow \eta \pi^+$ branching ratios. Note nevertheless that they are known to be close to unity because they are dominant decay modes.

We obtain:

$$\begin{aligned}
 \mathcal{B}(\bar{B}^0 \rightarrow \pi^+ \ell \bar{\nu}) &= (0.89 \pm 0.34(\text{stat.}) \pm 0.12(\text{sys.})) \times 10^{-4}, \\
 \mathcal{B}(B^- \rightarrow \pi^0 \ell \bar{\nu}) &= (0.91 \pm 0.28(\text{stat.}) \pm 0.14(\text{sys.})) \times 10^{-4}, \\
 \mathcal{B}(\bar{B}^0 \rightarrow \rho^+ \ell \bar{\nu}) &= (3.5 \pm 1.1(\text{stat.}) \pm 0.7(\text{sys.})) \times 10^{-4}, \\
 \mathcal{B}(B^- \rightarrow \rho^0 \ell \bar{\nu}) &= (1.04 \pm 0.39(\text{stat.}) \pm 0.16(\text{sys.})) \times 10^{-4}, \\
 \mathcal{B}(B^- \rightarrow \omega \ell \bar{\nu}) &= (1.26 \pm 0.55(\text{stat.}) \pm 0.24(\text{sys.})) \times 10^{-4}, \\
 \mathcal{B}(B^- \rightarrow \eta \ell \bar{\nu}) &= (0.39 \pm 0.41(\text{stat.}) \pm 0.22(\text{sys.})) \times 10^{-4}, \\
 \mathcal{B}(B^- \rightarrow \eta' \ell \bar{\nu}) &= (2.7 \pm 1.2(\text{stat.}) \pm 0.5(\text{sys.})) \times 10^{-4}, \\
 \mathcal{B}(B^- \rightarrow a_0^0 \ell \bar{\nu}) \mathcal{B}(a_0^0 \rightarrow \eta \pi^0) &= (2.7 \pm 1.4(\text{stat.}) \pm 0.9(\text{sys.})) \times 10^{-4}, \\
 \mathcal{B}(\bar{B}^0 \rightarrow a_0^+ \ell \bar{\nu}) \mathcal{B}(a_0^+ \rightarrow \eta \pi^+) &= (0.7 \pm 1.6(\text{stat.}) \pm 0.3(\text{sys.})) \times 10^{-4},
 \end{aligned} \tag{15}$$

where the errors on $\mathcal{B}(\bar{B} \rightarrow X \ell \bar{\nu})$ are added in quadrature.

The rates for exclusive decays involving π^+ and π^0 and ρ^+ , ρ^0 , and ω can be constrained by the following isospin and quark model relations:

$$\begin{aligned}
 \Gamma(\bar{B} \rightarrow \pi \ell \bar{\nu}) &\equiv \Gamma(\bar{B}^0 \rightarrow \pi^+ \ell \bar{\nu}) = 2\Gamma(B^- \rightarrow \pi^0 \ell \bar{\nu}) \\
 \Gamma(\bar{B} \rightarrow \rho \ell \bar{\nu}) &\equiv \Gamma(\bar{B}^0 \rightarrow \rho^+ \ell \bar{\nu}) = 2\Gamma(B^- \rightarrow \rho^0 \ell \bar{\nu}) \\
 \Gamma(B^- \rightarrow \omega \ell \bar{\nu}) &= \Gamma(B^- \rightarrow \rho^0 \ell \bar{\nu})
 \end{aligned} \tag{16}$$

and it is possible to combine the results. Using a lifetime ratio of $\frac{\tau_{B^+}}{\tau_{B^0}} = 1.086 \pm 0.017$ we obtain:

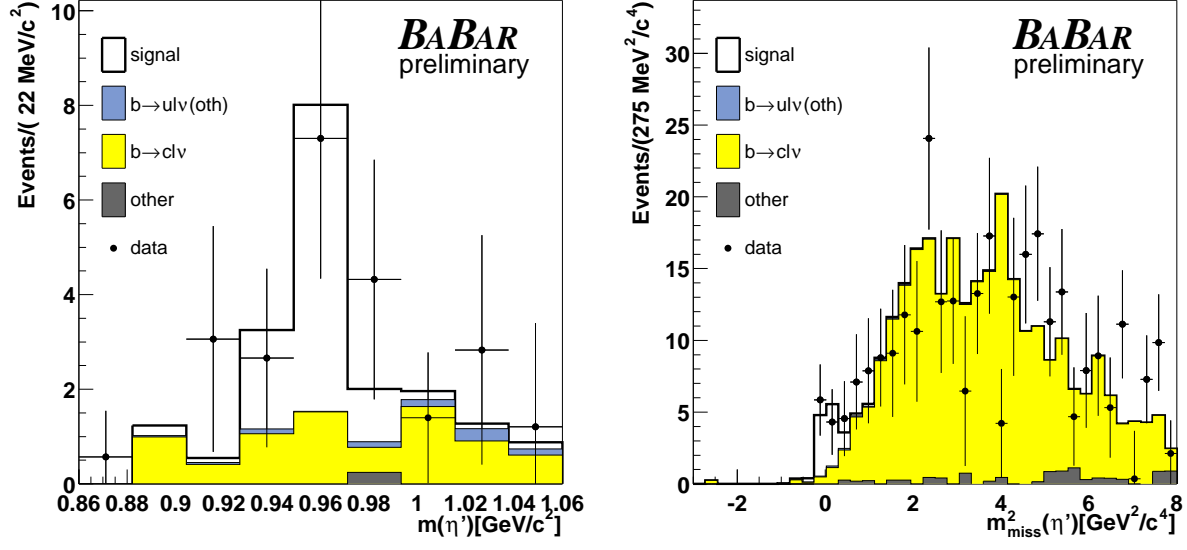


Figure 17: $B^- \rightarrow \eta' \ell \bar{\nu}$: Projection of the fit result onto the $m(\eta')$ (left) and $m_{miss}^2(\eta')$ (right) variables.

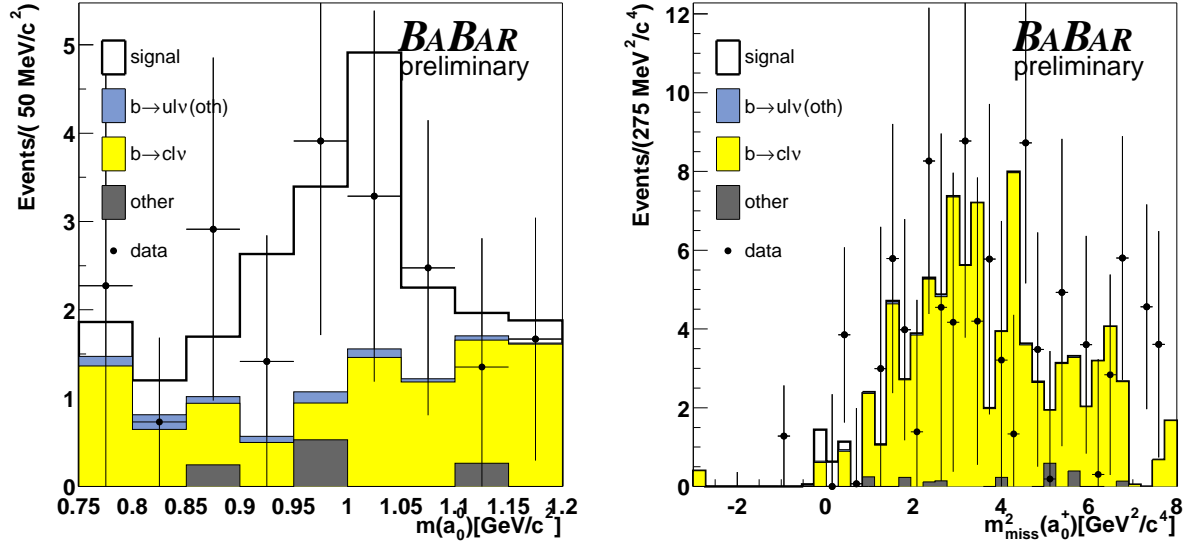


Figure 18: $B^- \rightarrow a_0^0 \ell \bar{\nu}$: Projection of the fit result onto the $m(a_0^0)$ (left) and $m_{miss}^2(a_0^0)$ (right) variables.

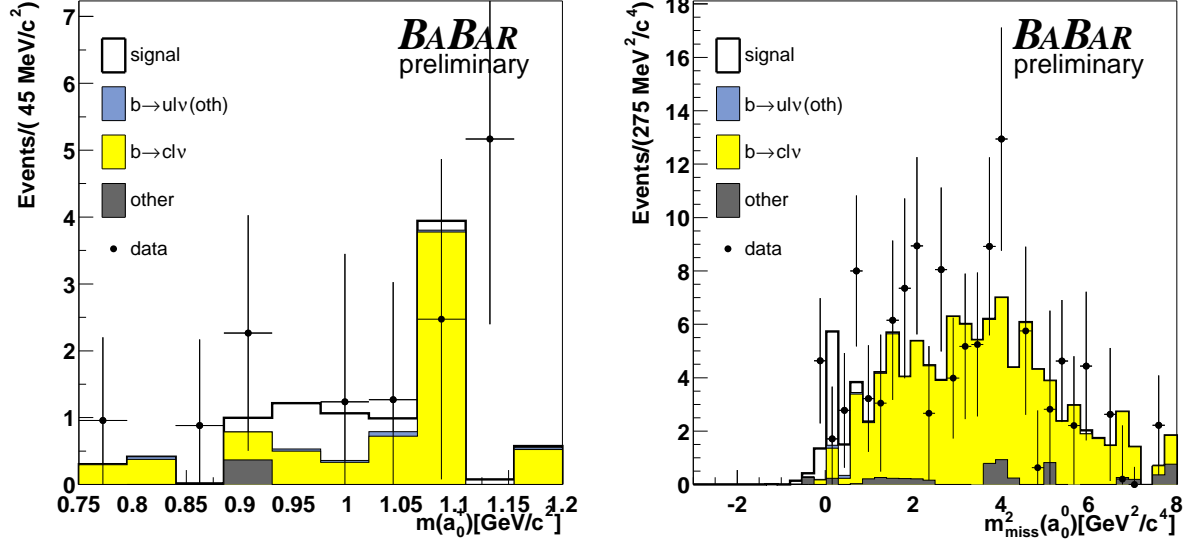


Figure 19: $\bar{B}^0 \rightarrow a_0^+ \ell \bar{\nu}$: Projection of the fit result onto the $m(a_0^+)$ (left) and $m_{miss}^2(a_0^+)$ (right) variables.

$$\begin{aligned} \mathcal{B}(\bar{B} \rightarrow \pi \ell \bar{\nu}) &= (1.08 \pm 0.28(\text{stat.}) \pm 0.16(\text{sys.}) \times 10^{-4}, \\ \mathcal{B}(\bar{B} \rightarrow \rho \ell \bar{\nu}) &= (2.57 \pm 0.52(\text{stat.}) \pm 0.59(\text{sys.}) \times 10^{-4}. \end{aligned} \quad (17)$$

We also set 90% C.L. upper limits on the $B^- \rightarrow \eta \ell \bar{\nu}$, $B^- \rightarrow \eta' \ell \bar{\nu}$, $B^- \rightarrow a_0^0 \ell \bar{\nu}$, and $\bar{B}^0 \rightarrow a_0^+ \ell \bar{\nu}$ branching fractions:

$$\begin{aligned} \mathcal{B}(B^- \rightarrow \eta \ell \bar{\nu}) &< 1.2 \times 10^{-4} \text{ (90\% C.L.)}, \\ \mathcal{B}(B^- \rightarrow \eta' \ell \bar{\nu}) &< 4.5 \times 10^{-4} \text{ (90\% C.L.)}, \\ \mathcal{B}(B^- \rightarrow a_0^0 \ell \bar{\nu}) \mathcal{B}(a_0^0 \rightarrow \eta \pi^0) &< 5.3 \times 10^{-4} \text{ (90\% C.L.)}, \\ \mathcal{B}(\bar{B}^0 \rightarrow a_0^+ \ell \bar{\nu}) \mathcal{B}(a_0^+ \rightarrow \eta \pi^+) &< 3.3 \times 10^{-4} \text{ (90\% C.L.)}. \end{aligned} \quad (18)$$

9 Conclusions

Preliminary results on charmless semileptonic B decays have been obtained on a sample of 88 million $\Upsilon(4S) \rightarrow B\bar{B}$ decays collected by the *BABAR* experiment at the PEP-II asymmetric-energy B factory at SLAC, in events in which one B meson decaying to a hadronic final state is fully reconstructed and the semileptonic decay of the second B meson is identified by the detection of a charged lepton.

We have explored several new approaches to the study of $\bar{B} \rightarrow X_u \ell \bar{\nu}$ decays, most of which are statistically limited and some of which are already competitive with the best existing measurements.

From the measurement of the spectrum of the invariant mass of the hadrons X_u (M_X) we derive the branching fraction

$$\mathcal{B}(\bar{B} \rightarrow X_u \ell \bar{\nu}) = (2.53 \pm 0.29(\text{stat.}) \pm 0.26(\text{sys.})_{-0.41}^{+0.69}(\text{theo.})) \times 10^{-3}. \quad (19)$$

From the two-dimensional distribution of M_X and q^2 , the squared invariant mass of the two leptons, we derive the partial branching fraction for $M_X < 1.7 \text{ GeV}/c^2$, $q^2 > 8 \text{ GeV}^2/c^4$ to be

$$\Delta\mathcal{B}(\bar{B} \rightarrow X_u \ell \bar{\nu}) = (0.88 \pm 0.14(\text{stat.}) \pm 0.13(\text{sys.}) \pm 0.02(\text{theo.})) \times 10^{-3}. \quad (20)$$

From these two measurements, utilizing the calculation of the fraction of events in the selected phase space region from DFN [5] and BLL [6] in the M_X and M_X - q^2 analysis respectively, we can extract

$$\begin{aligned} |V_{ub}|_{M_X} &= (4.77 \pm 0.28(\text{stat.}) \pm 0.28(\text{sys.})_{-0.45}^{+0.69}(\text{theo.})) \times 10^{-3} \quad \text{and} \\ |V_{ub}|_{M_X-q^2} &= (4.92 \pm 0.39(\text{stat.}) \pm 0.36(\text{sys.}) \pm 0.46(\text{theo.})) \times 10^{-3}, \end{aligned} \quad (21)$$

respectively. These results are competitive with the current world average ⁷ $|V_{ub}| = (4.57 \pm 0.61) \times 10^{-3}$.

The theoretical error is dominated by the uncertainty on the shape function parameters. In the process of writing this paper we were informed of an improved determination of these parameters from the photon energy spectrum measured by Belle in $b \rightarrow s\gamma$ decays (see Sec. 2.1). Utilizing these new constraints on the shape function parameters we get

$$\begin{aligned} |V_{ub}|_{M_X} &= (5.22 \pm 0.30(\text{stat.}) \pm 0.31(\text{sys.})_{-0.32}^{+0.33}(\text{theo.})) \times 10^{-3} \\ |V_{ub}|_{M_X-q^2} &= (4.98 \pm 0.40(\text{stat.}) \pm 0.39(\text{sys.}) \pm 0.47(\text{theo.})) \times 10^{-3}, \end{aligned} \quad (22)$$

to be compared with the measured values of $|V_{ub}|$ in Eq. 21. These results show that the determination of the shape function parameters is critical to these measurements. Furthermore the two approaches deal differently with the shape function parameterizations: in particular the BLL approach does not correct the acceptance for shape function effects but assigns a large error. The corresponding result is therefore more stable but returns a worse error than the DFN approach in case of accurate determinations of the shape function parameters.

On the other side, the dependence of the $|V_{ub}|$ measurement as a function of the requirement on q^2 (Fig. 8) shows that both models reproduce the signal q^2 distribution well.

The reconstructed M_X spectrum is also used to unfold the M_X distribution for $\bar{B} \rightarrow X_u \ell \bar{\nu}$ events and to measure its first and second moments (see Table 1). With a higher statistics data sample, these measurements can be used to constrain the shape function parameters.

From the same data sample, several exclusive charmless semileptonic B decays are identified and their branching fractions measured (see Sec. 8.4). Imposing isospin and quark-model relationships we derive:

$$\begin{aligned} \mathcal{B}(\bar{B} \rightarrow \pi \ell \bar{\nu}) &= (1.08 \pm 0.28(\text{stat.}) \pm 0.16(\text{sys.})) \times 10^{-4} \quad , \\ \mathcal{B}(\bar{B} \rightarrow \rho \ell \bar{\nu}) &= (2.57 \pm 0.52(\text{stat.}) \pm 0.59(\text{sys.})) \times 10^{-4} \quad . \end{aligned}$$

Although these measurements are still statistically limited, the signal samples are very clean and are selected with very loose criteria which will allow the measurement of form factors with somewhat larger data samples. We are grateful for the extraordinary contributions of our PEP-II

⁷See the HFAG page <http://www.slac.stanford.edu/xorg/hfag/semi/winter04/winter04.shtml> .

colleagues in achieving the excellent luminosity and machine conditions that have made this work possible. The success of this project also relies critically on the expertise and dedication of the computing organizations that support *BABAR*. The collaborating institutions wish to thank SLAC for its support and the kind hospitality extended to them. This work is supported by the US Department of Energy and National Science Foundation, the Natural Sciences and Engineering Research Council (Canada), Institute of High Energy Physics (China), the Commissariat à l’Energie Atomique and Institut National de Physique Nucléaire et de Physique des Particules (France), the Bundesministerium für Bildung und Forschung and Deutsche Forschungsgemeinschaft (Germany), the Istituto Nazionale di Fisica Nucleare (Italy), the Foundation for Fundamental Research on Matter (The Netherlands), the Research Council of Norway, the Ministry of Science and Technology of the Russian Federation, and the Particle Physics and Astronomy Research Council (United Kingdom). Individuals have received support from CONACyT (Mexico), the A. P. Sloan Foundation, the Research Corporation, and the Alexander von Humboldt Foundation.

A The Unfolded Spectrum and the Covariance Matrix

Table 7: Fraction of $\bar{B} \rightarrow X_u \ell \bar{\nu}$ events measured in a given bin i of Fig. 6 and corresponding breakdown of errors. All numbers are in percent.

i	x_{unf}^i	σ^i	$\sigma_{\text{stat}}^i \oplus \sigma_{\text{MCstat}}^i$	σ_{det}^i	$\sigma_{\text{ul}\nu}^i \oplus \sigma_{\text{theo}}^i$	$\sigma_{\text{bkg}}^i \oplus \sigma_{\text{breco}}^i$
1	2.890	1.655	1.206	0.589	0.322	0.423
2	1.067	1.294	0.895	0.415	0.685	0.266
3	5.355	4.039	3.325	0.906	0.952	1.026
4	9.840	4.934	3.532	1.388	1.999	1.537
5	28.024	8.330	5.302	2.807	3.111	4.183
6	25.830	3.657	1.850	1.223	1.169	2.377
7	15.880	5.996	3.964	1.806	2.742	1.872
8	7.189	5.742	3.935	1.940	1.161	2.998
9	2.742	4.213	2.534	1.276	1.939	2.209
10	0.880	1.822	1.194	0.627	0.290	1.097
11	0.261	0.737	0.478	0.260	0.104	0.451
12	0.038	0.149	0.088	0.064	0.036	0.084
13	0.002	0.018	0.006	0.011	0.008	0.006
14	0.001	0.005	0.002	0.003	0.002	0.002
15	0.000	0.001	0.000	0.000	0.000	0.000
16	0.000	0.000	0.000	0.000	0.000	0.000

Table 8: Full covariance matrix on the fraction of $\bar{B} \rightarrow X_u \ell \bar{\nu}$ in the unfolded M_X spectrum (as in Table 7)). All numbers are in 10^{-4} .
A version with a higher number of digits can be obtained from the authors.

2.739	1.021	4.254	5.685	8.257	-1.605	-7.474	-6.267	-4.099	-1.734	-0.647	-0.117	-0.010	-0.003	-0.000	-0.000
1.021	1.674	2.975	3.853	4.058	-0.992	-4.398	-4.012	-2.465	-1.153	-0.460	-0.091	-0.009	-0.003	-0.000	-0.000
4.254	2.975	16.314	13.999	17.275	-5.302	-17.648	-15.958	-9.264	-4.448	-1.802	-0.351	-0.033	-0.009	-0.002	-0.001
5.685	3.853	13.999	24.343	34.115	-1.585	-28.030	-24.898	-17.030	-7.222	-2.692	-0.484	-0.039	-0.012	-0.002	-0.001
8.257	4.058	17.275	34.115	69.389	11.837	-45.085	-45.370	-33.773	-14.300	-5.325	-0.965	-0.082	-0.025	-0.004	-0.002
-1.605	-0.992	-5.302	-1.585	11.837	13.373	-0.222	-5.212	-6.439	-2.675	-0.980	-0.176	-0.015	-0.005	-0.001	-0.000
-7.474	-4.398	-17.648	-28.030	-45.085	-0.222	35.949	31.214	22.623	9.146	3.289	0.574	0.045	0.014	0.002	0.001
-6.267	-4.012	-15.958	-24.898	-45.370	-5.212	31.214	32.971	22.363	10.272	4.042	0.763	0.067	0.020	0.003	0.002
-4.099	-2.465	-9.264	-17.030	-33.773	-6.439	22.623	22.363	17.751	7.207	2.603	0.466	0.041	0.012	0.002	0.001
-1.734	-1.153	-4.448	-7.222	-14.300	-2.675	9.146	10.272	7.207	3.319	1.309	0.249	0.022	0.007	0.001	0.001
-0.647	-0.460	-1.802	-2.692	-5.325	-0.980	3.289	4.042	2.603	1.309	0.543	0.107	0.010	0.003	0.001	0.000
-0.117	-0.091	-0.351	-0.484	-0.965	-0.176	0.574	0.763	0.466	0.249	0.107	0.022	0.002	0.001	0.000	0.000
-0.010	-0.009	-0.033	-0.039	-0.082	-0.015	0.045	0.067	0.041	0.022	0.010	0.002	0.000	0.000	0.000	0.000
-0.003	-0.003	-0.009	-0.012	-0.025	-0.005	0.014	0.020	0.012	0.007	0.003	0.001	0.000	0.000	0.000	0.000
-0.000	-0.000	-0.002	-0.002	-0.004	-0.001	0.002	0.003	0.002	0.001	0.001	0.000	0.000	0.000	0.000	0.000
-0.000	-0.000	-0.001	-0.001	-0.002	-0.000	0.001	0.002	0.001	0.001	0.000	0.000	0.000	0.000	0.000	0.000

References

- [1] BABAR, B. Aubert *et al.*, Phys. Rev. Lett. **92**, 071802 (2004).
- [2] C. W. Bauer and A. V. Manohar, “Shape function effects in $B \rightarrow X_s \gamma$ and $B \rightarrow X_u l \nu$ decays”, hep-ph/0312109.
- [3] S. W. Bosch, B. O. Lange, M. Neubert and G. Paz, “Proposal for a precision measurement of $|V(ub)|$ ”, hep-ph/0403223.
- [4] L. Gibbons, “The status of $|V(ub)|$ ”, hep-ex/0402009.
- [5] F. De Fazio and M. Neubert, JHEP **06**, 017 (1999).
- [6] C. W. Bauer, Z. Ligeti and M. Luke, “Precision determination of $V(ub)$ ”, hep-ph/0111387.
- [7] BABAR, B. Aubert *et al.*, Nucl. Instrum. Meth. **A479**, 1 (2002).
- [8] GEANT4, S. Agostinelli *et al.*, Nucl. Instrum. Meth. **A506**, 250 (2003).
- [9] CLEO, D. Cronin-Hennessy *et al.*, Phys. Rev. Lett. **87**, 251808 (2001).
- [10] T. Sjostrand, “High-energy physics event generation with PYTHIA 5.7 and JETSET 7.4”, Comput. Phys. Commun. **82**, 74 (1994).
- [11] N. Isgur and D. Scora, Phys. Rev. D **52**, 2783 (1995).
- [12] A. Limosani and T. Nozaki, “Extraction of the b -quark shape function parameters using the Belle $B \rightarrow X_s \gamma$ photon energy spectrum.”, hep-ex/0407052.
- [13] CLEO, J. E. Duboscq *et al.*, Phys. Rev. Lett. **76**, 3898 (1996).
- [14] J. L. Goity and W. Roberts, Phys. Rev. **D51**, 3459 (1995).
- [15] ARGUS, H. Albrecht *et al.*, Phys. Lett. **B318**, 397 (1993).
- [16] Crystal Ball, T. Skwarnicki, “A Study of the Radiative Cascade Transitions Between the Υ' and Υ Resonances”, DESY F31-86-02, Ph.D. thesis.
- [17] BABAR, B. Aubert *et al.*, Phys. Rev. Lett **93**, 011803 (2004).
- [18] Particle Data Group, K. Hagiwara *et al.*, Phys. Rev. **D66**, 010001 (2002).
- [19] Particle Data Group, S. Eidelman *et al.*, Physics Letters B **592**, 1 (2004).
- [20] A. Hoecker and V. Kartvelishvili, Nucl. Instrum. Meth. **A372**, 469 (1996).
- [21] E852, S. Teige *et al.*, Phys. Rev. **D59**, 012001 (1999).
- [22] CLEO, S. B. Athar *et al.*, Phys. Rev. **D68**, 072003 (2003).